AIAA SciTech
5-9 January 2015, Kissimmee, Florida
AIAA Guidance, Navigation, and Control Conference

Attitude Control and Stabilization of Spacecraft with a Captured Asteroid

Saptarshi Bandyopadhyay*, Soon-Jo Chung†
University of Illinois at Urbana-Champaign, Urbana, Illinois, 61801, USA
and
Fred Y. Hadaegh‡
Jet Propulsion Laboratory, California Institute of Technology, Pasadena, California 91109, USA

National Aeronautics and Space Administration's Asteroid Redirect Mission (ARM) aims to capture a Near Earth Orbit (NEO) asteroid or a piece of a large asteroid and transport it to the Earth–Moon system. In this paper, we provide a detailed analysis of one of the main control challenges for the first ARM mission concept, namely despinning and three-axis stabilizing the asteroid and spacecraft combination after the ARM spacecraft captures the tumbling NEO asteroid. We first show that control laws, which explicitly use the dynamics of the system in their control law equation, encounter a fundamental limitation due to modeling uncertainties. We show that in the presence of large modeling uncertainties, the resultant disturbance torque for such control laws may well exceed the maximum control torque of the conceptual ARM spacecraft. We then numerically compare the performance of three viable control laws: the robust nonlinear tracking control law, the adaptive nonlinear tracking control law, and the simple derivative plus proportional-derivative linear control strategy. We conclude that under very small modeling uncertainties, which can be achieved using online system identification, the robust nonlinear tracking control law guarantees exponential convergence to the fuel-optimal reference trajectory and hence consumes the least fuel. On the other hand, in the presence of large modeling uncertainties, measurement errors, and actuator saturations, the best strategy for stabilizing the asteroid and spacecraft combination is to first despin the system using a derivative (rate damping) linear control law and then stabilize the system in the desired orientation using the simple proportional-derivative linear control law. Moreover, the fuel consumed by the conceptual ARM spacecraft using these control strategies is upper bounded by 300 kg for the nominal range of NEO asteroid parameters. We conclude this paper with specific design guidelines for the ARM spacecraft for efficiently stabilizing the tumbling NEO asteroid and spacecraft combination.

Nomenclature

$\boldsymbol{B}$	=	Control influence matrix ($\boldsymbol{B} \in \mathbb{R}^{3\times 8}$)
B_{CM}	=	Center of mass of the asteroid and spacecraft combination
$\boldsymbol{C}(\boldsymbol{q},\dot{\boldsymbol{q}})$, $\hat{\boldsymbol{C}}(\hat{\boldsymbol{q}},\dot{\hat{\boldsymbol{q}}})$	=	Damping terms in Euler–Lagrangian formulation
$\mathcal{F}_I$	=	Inertial frame
$\mathcal{F}_B$	=	Body frame
$\mathcal{F}_S$	=	Spacecraft frame
$\mathbf{I}$	=	Identity matrix
I_{sp}	=	Specific impulse of the fuel

*Graduate Research Assistant, Department of Aerospace Engineering, bandyop2@illinois.edu.
†Assistant Professor, Department of Aerospace Engineering and Coordinated Science Laboratory, sjchung@illinois.edu. Senior Member AIAA.
‡Senior Research Scientist and Technical Fellow; fred.y.hadaegh@jpl.nasa.gov. Fellow AIAA.

$\boldsymbol{J}_{\text{ast}}^{B_{CM}}$, $\hat{\boldsymbol{J}}_{\text{ast}}^{B_{CM}}$ = Inertia tensors of the asteroid at B_{CM} in $\mathcal{F}_B$
$\boldsymbol{J}_{\text{sc}}^{S_{CM}}$ = Inertia tensor of the ARM spacecraft at S_{CM} in $\mathcal{F}_S$
$\boldsymbol{J}_{\text{tot}}^{B_{CM}}$, $\hat{\boldsymbol{J}}_{\text{tot}}^{B_{CM}}$ = Inertia tensors of the asteroid and spacecraft combination at B_{CM} in $\mathcal{F}_B$
$\boldsymbol{K}_r$, $\boldsymbol{\Lambda}_r$, $\boldsymbol{\Gamma}_r$, $\boldsymbol{K}_d$, k_p = Control law gains
$\boldsymbol{M}(\boldsymbol{q})$, $\hat{\boldsymbol{M}}(\hat{\boldsymbol{q}})$ = Inertia matrices in Euler–Lagrangian formulation
$\mathcal{P}(\cdot)$ = Height of the power spectral density of the white noise
P_i = Thruster pods ($i = \{1, 2, 3, 4\}$)
$\boldsymbol{R}$ = Rotation Matrix ($\boldsymbol{R} \in \mathbb{R}^{3\times3}$)
$\mathbb{R}$ = Real numbers
S_{CM} = Center of mass of the ARM spacecraft
S_O = Base of the ARM-spacecraft's body
$\mathbb{S}^2$ = Two-sphere ($\{(x_1, x_2, x_3) \in \mathbb{R}^3 : \|(x_1, x_2, x_3)\| = 1\}$)
$\mathbb{S}^3$ = Three-sphere ($\{(x_1, x_2, x_3, x_4) \in \mathbb{R}^4 : \|(x_1, x_2, x_3, x_4)\| = 1\}$)
SO(3) = Special orthogonal group ($\{\boldsymbol{R} \in \mathbb{R}^{3\times3} : \boldsymbol{R}\boldsymbol{R}^T = \boldsymbol{R}^T\boldsymbol{R} = \mathbf{I}, \det(\boldsymbol{R}) = 1\}$)
V_d, V_{pd} = Lyapunov functions
$\boldsymbol{d}_{\text{ext}}$ = External disturbance torque
$\boldsymbol{d}_{\text{res}}$, $\tilde{\boldsymbol{d}}_{\text{res}}$ = Resultant disturbance torques
$\boldsymbol{e}$, Φ = Euler Axis of Rotation ($\boldsymbol{e} \in \mathbb{R}^3$) and Angle ($\Phi \in \mathbb{R}^1$, rad)
g_0 = Nominal acceleration due to the gravity (9.8 m sec^{-2})
m_{ast} = Mass of asteroid (kg)
m_{sc} = Mass of spacecraft (kg)
$\boldsymbol{q}$ = Modified Rodrigues Parameters ($\boldsymbol{q} \in \mathbb{R}^3$)
$\boldsymbol{r}^{B/A}$ = Vector from A to B
$\hat{s}_x$, $\hat{s}_y$, $\hat{s}_z$ = Unit vectors in $\mathcal{F}_S$
$\boldsymbol{u}$ = Thrust output ($\boldsymbol{u} \in \mathbb{R}^8$)
$\Delta(\cdot)$ = Modeling, measurement or actuator error
$\boldsymbol{\beta}$ = Quaternions ($\boldsymbol{\beta} \in \mathbb{R}^4$)
$\varepsilon_{\text{trans}}$, ε_{ss} = Transient and steady-state errors
λ = Eigenvalue
ρ_{ast} = Density of asteroid (g cm^{-3})
$\boldsymbol{\sigma}$ = Classical Rodrigues Parameters ($\boldsymbol{\sigma} \in \mathbb{R}^3$)
$\boldsymbol{\tau}_c$, $\hat{\boldsymbol{\tau}}_c$ = Control terms in Euler–Lagrangian formulation
$\boldsymbol{\tau}_{\text{ext}}$, $\boldsymbol{\tau}_{\text{res}}$ = Disturbance terms in Euler–Lagrangian formulation
ϕ, θ, ψ = Euler Angles (ϕ, θ, $\psi \in \mathbb{R}^1$, rad)
$\boldsymbol{\omega}$ = Angular velocity ($\boldsymbol{\omega} \in \mathbb{R}^3$, rad sec^{-1})
$\|\cdot\|_p$ = p-vector norm or matrix norm
$(\cdot)^S$ = Shadow point representation

I. Introduction

Multiple space agencies have announced plans for future small body exploration and hazard mitigation missions.[1,2,3] Recently, European Space Agency's Rosetta spacecraft landed the Philae robotic lander on the nucleus of the comet 67P/Churyumov–Gerasimenko on November 12, 2014.[4] National Aeronautics and Space Administration's (NASA) Asteroid Redirect Mission (ARM) is targeting carbonaceous Near Earth Orbit (NEO) asteroids, which have diameters between 7-10 m and mass between 2.5-13 $\times$ 10^5 kg, as they could potentially answer questions about the origin of life and provide opportunities for in-situ resource utilization.[5,6,7] The objective of the first ARM mission concept is to capture a NEO asteroid in deep space and transport the captured asteroid back to the Earth–Moon system. The conceptual ARM spacecraft design shown in Fig. 1(a) is proposed for this mission, which weighs 15,500 kg and carries a 40 kW solar

electric propulsion (SEP) system.[8] In this paper, we provide a detailed analysis of one of the main control challenges for this ARM mission concept: despinning and three-axis stabilizing the asteroid and spacecraft combination after the tumbling asteroid is captured by the ARM spacecraft. In case a suitable NEO asteroid is not found, an alternate ARM mission concept is to pick up a rock from a much larger asteroid.[9,10] This alternate ARM mission concept is not considered in this study.

(a) (b)

Figure 1: (a) Artist's rendering of the conceptual ARM spacecraft about to capture an asteroid (image credit: NASA[11]). (b) Artist's rendering of the Orion spacecraft about to dock with the conceptual ARM spacecraft with the captured asteroid (image credit: NASA[12]).

In this paper, we consider the first ARM mission concept; i.e., the ARM spacecraft intends to capture the NEO asteroid and transport in to the Earth–Moon system. In Refs. 13,14, a number of target NEO asteroids are identified for this ARM mission concept. Trajectories for intercepting these NEO asteroid and returning with the captured asteroid to the Earth–Moon system, using the 40 kW SEP system onboard the conceptual ARM spacecraft, are discussed in Refs. 15,16. After reaching the chosen NEO asteroid, the ARM spacecraft will perform proximity operations to estimate the asteroid's physical parameters like angular velocity (spin rate), shape, mass, center of mass, inertia tensor, etc.[17,18,19] Note that these physical parameters of the chosen NEO asteroid cannot be precisely determined from Earth-based observations, hence the ARM spacecraft should be capable of dealing with a wide range of asteroid parameters. However, the captured asteroid's physical parameters could be precisely estimated using online system identification techniques.[20,21,22,23,24] Strategies for initial approach, inertial hovering, and body-fixed hovering are discussed in Refs. 25,26,27. In order to capture the NEO asteroid, the ARM spacecraft would first match the asteroid's rotation, capture it using the capture mechanism, secure it firmly to the spacecraft's body, and then propulsively despin the combination. Some of the capture mechanisms that have been conceptualized for the ARM spacecraft are the inflatable ribs and bag concept shown in Fig. 1 and flexible capture mechanisms.[9,28] The ARM spacecraft with the captured asteroid would then depart the asteroid's original orbit, return to the vicinity of the Earth–Moon system, and enter a Lunar distant retrograde orbit. A manned Orion spacecraft would later rendezvous with the ARM spacecraft and astronauts would set foot on the captured asteroid, as depicted in Fig. 1(b).

The focus of this paper is to develop attitude control strategies for despinning and three-axis stabilizing the asteroid and spacecraft combination after the tumbling asteroid is captured by the ARM spacecraft. In Refs. 29, 30, a simple attitude control strategy is presented that assumes perfect knowledge of the asteroid's physical parameters and neglects modeling uncertainties and disturbances. In contrast, we develop attitude control strategies that stabilize the tumbling asteroid and spacecraft combination in the presence of uncertain physical parameters, bounded disturbances, measurement errors, and actuator saturations. Nonlinear adaptive control strategies for attitude stabilization of spacecraft with uncertain inertia tensor are discussed in Refs. 31,32,33,34,35. In Refs. 36,37,38,39,40, sliding mode control or robust $\mathcal{H}_\infty$ control is used for attitude stabilization of spacecraft with uncertainties and disturbances. In this paper, we show that control laws, which use the dynamics of the system in the control law equation, experience a large resultant disturbance torque due to modeling uncertainties. In contrast, control laws, which do not use the dynamics of the system in the control law equation,[41,42,43,44] experience a much smaller resultant disturbance torque. We show that in the presence of large modeling uncertainties, measurement errors, and actuator saturations, the best control strategy is to first despin the system using a derivative (rate damping) linear control law and then stabilize the system in the desired orientation using the simple proportional-derivative linear control

law. On the other hand, the best control strategy under very small modeling uncertainties is to track the fuel-optimal reference trajectory using the globally-exponentially-stabilizing robust nonlinear tracking control law. We also present specific design guidelines for the ARM spacecraft based on these attitude control strategies.

A. Paper Contribution and Organization

Section II discusses the problem statement and some preliminaries. We first present a brief introduction of NEO asteroids and the conceptual ARM spacecraft in Section II.A. The attitude kinematics and dynamics of the asteroid and spacecraft combination and its Euler–Lagrangian formulation using modified Rodrigues parameters are presented in Section II.B. The control problem statement of this paper is presented in Section II.C.

The first main contribution of this paper, discussed in Section III, is the fundamental limit of control laws that use the dynamics of the system in the control law equation. We show that the resultant disturbance torque, due to modeling uncertainties, for such control laws is comparable to the maximum control torque of the conceptual ARM spacecraft. Therefore such control laws are unsuitable for this control problem in the presence of large modeling uncertainties. In contrast, the resultant disturbance torque is much smaller for control laws that do not use the dynamics of the system in the control law equation.

In Section IV, we present three control laws for this control problem, namely the robust nonlinear tracking control law (Section IV.A), the adaptive nonlinear tracking control law (Section IV.B), and the derivative plus proportional-derivative linear control strategy (Section IV.C). The comparison of these control laws using numerical simulations, in terms of fuel usage and time of convergence, is presented in Section V.

The second main contribution of this paper is recognizing that in the presence of large modeling uncertainties, measurement errors, and actuator saturations, the best control strategy is to first despin the system using a derivative (rate damping) linear control law and then stabilize the system in the desired orientation using the simple proportional-derivative linear control law. On the other hand, the best control strategy under very small modeling uncertainties, which can be achieved using online system identification from both proximity and contact operations, is to track the fuel-optimal reference trajectory using the globally-exponentially-stabilizing robust nonlinear tracking control law. We show that the fuel consumed by the conceptual ARM spacecraft using these control strategies is upper bounded by 300 kg for the nominal range of asteroid parameters. Finally, in Section VI, we provide specific design guidelines for the ARM spacecraft for efficiently stabilizing the asteroid and spacecraft combination.

II. Preliminaries and Problem Statement

In this section, we first present a brief introduction of the conceptual ARM spacecraft and potential NEO asteroid targets. We then present the attitude kinematics and dynamics of the asteroid and spacecraft combination and finally introduce the problem statement.

A. Conceptual ARM Spacecraft Design and NEO Asteroid Parameters

As stated earlier, the first ARM mission concept aims to bring a small NEO asteroid into the Earth–Moon system, where it could be further analyzed by a future manned mission. Feasibility studies for the ARM mission have identified the challenges and enabling technologies for this mission.[5,6,7] According to these studies, the most desirable asteroids are the carbonaceous C–type asteroids because samples from these asteroids can return to Earth without any restriction.[6] The densities of asteroids can range from 1 g cm^{-3} for a high-porosity carbonaceous chondrite to 8 g cm^{-3} for solid nickel-iron meteorites, but the majority of NEO asteroids have densities between 1.9-3.8 g cm^{-3}. It is estimated that C–type NEO asteroids with 7-10 m diameter would be in the 2.5-13 $\times$ 10^5 kg mass range.[6] Table 1 lists the nominal range of NEO asteroid parameters that the ARM spacecraft should be capable of handling.

The constraint on the initial angular velocity (spin rate) of the tumbling asteroid results from the technological capability of the sensors and angular momentum capacity of the actuators to be used onboard the ARM spacecraft. In order to generate realistic models of asteroids for numerical simulations, we use the shape models of the asteroids 433 Eros[45] and 25143 Itokawa[46] shown in Fig. 2(a,b). Multiple models of asteroids are generated by sizing these shape models using the physical parameters given in Table 1. For example, the diameters of these realistic asteroid models are shown in Fig. 2(c,d). Figures 2(c,d) also show

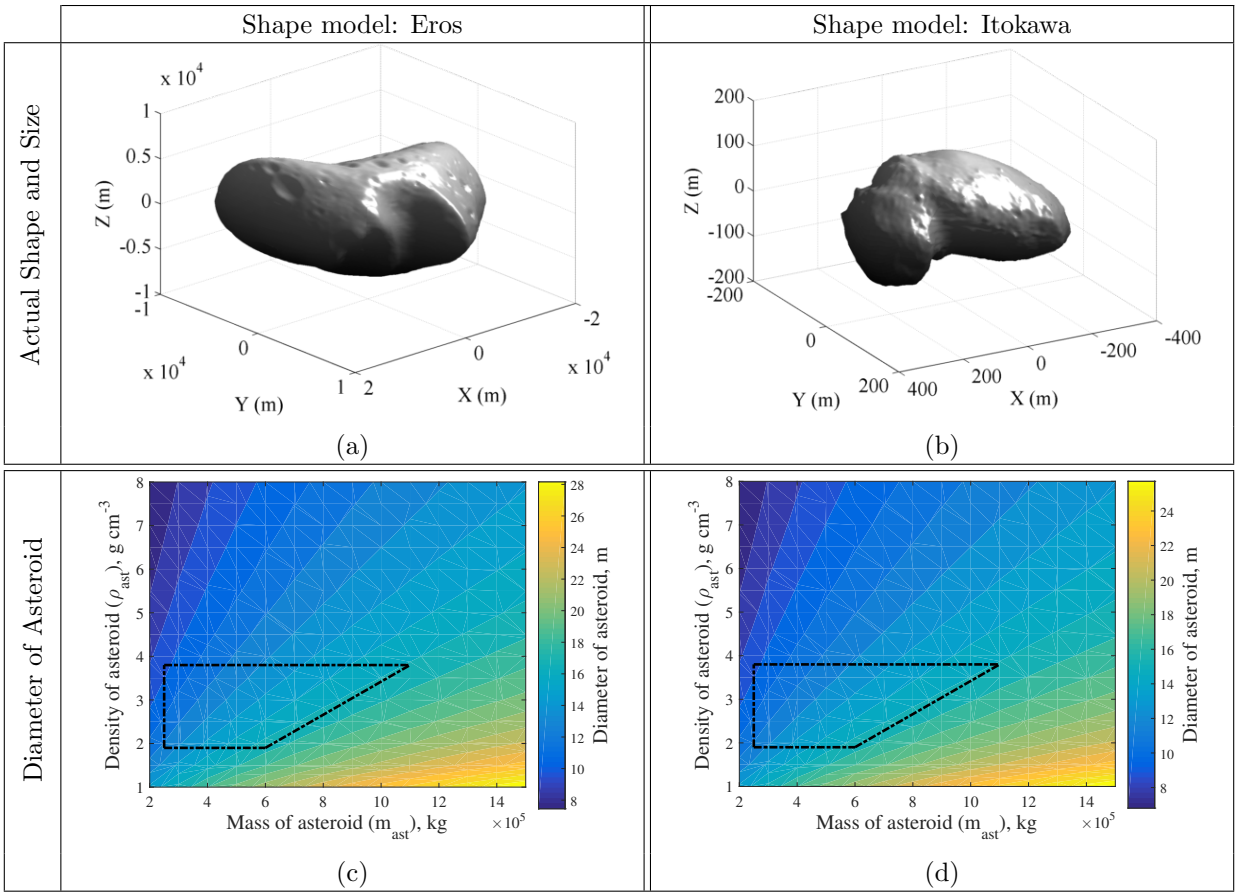

Figure 2: Shape models of asteroids (a) 433 Eros[45] and (b) 25143 Itokawa[46] are used for generating realistic models of asteroids. In (c,d), the diameters of realistic asteroid models are shown, which are obtained by sizing the shape models of Eros and Itokawa respectively for the given masses and densities. The inset black trapezium shows the nominal range of NEO asteroid parameters, where the asteroid's mass is within 2.5-13 $\times 10^5$ kg, the asteroid's density is within 1.9-3.8 g cm^{-3}, and the asteroid's diameter is less than 15 m.

the nominal range of NEO asteroid parameters considered for this ARM mission concept, i.e., the asteroid's mass is within 2.5-13 $\times 10^5$ kg, the asteroid's density is within 1.9-3.8 g cm^{-3}, and the asteroid's diameter is less than 15 m. It is seen that asteroids with large mass and small density have large diameters and consequently have large moments of inertia. These realistic models of asteroids are used for Monte Carlo simulations in Section V for comparing the various control laws discussed in this paper.

A conceptual design of the ARM spacecraft is shown in Fig. 3(a), which is used as the nominal ARM spacecraft design in this paper. This conceptual ARM spacecraft, with dry mass of 5,500 kg and wet mass of 15,500 kg, could carry 13×10^3 kg of Xenon propellant for the 40 kW SEP system and an additional 900 kg of liquid propellant for the roll control thrusters.[8] The various propulsion systems on board the conceptual ARM spacecraft are shown in Fig. 3(b). The SEP system includes five Hall thrusters and power processor units. The SEP system will be used by the conceptual ARM spacecraft for the journey to the chosen NEO asteroid and also for bringing the captured asteroid to the Earth–Moon system.[15,16] Attitude control during the SEP thrusting stage will be achieved by gimbaling the Hall thrusters.

On reaching the chosen NEO asteroid, the ARM spacecraft will perform proximity operations to estimate the asteroid's physical parameters like angular velocity (spin rate), mass, center of mass, inertia tensor, etc. In order to capture the tumbling NEO asteroid, the ARM spacecraft will first propulsively spin-up to match its angular velocity with that of the tumbling asteroid, i.e., remove the relative angular velocity between itself and the tumbling asteroid. The ARM spacecraft will then capture the asteroid using its capture mechanism. Note that there might be some slippage between the capture mechanism and the NEO asteroid, but we

Table 1: Nominal range of NEO asteroid parameters considered for the ARM mission[6]

Parameter	Range
Mass (m_{ast})	2.5-13 $\times$ 10^5 kg
Density (ρ_{ast})	1-8 g cm^{-3} (majority within 1.9-3.8 g cm^{-3})
Diameter	2-10 m
Initial Angular Velocity ($\boldsymbol{\omega}_{\text{initial}}$)	$\leq$ 0.5 rotations per minute (rpm)
Initial Attitude ($\boldsymbol{\beta}_{\text{initial}}$)	any attitude ($\boldsymbol{\beta}_{\text{initial}} \in \mathbb{S}^3$)

neglect it in this paper. The captured NEO asteroid and the ARM spacecraft will finally form a tumbling rigid body.

The Reaction Control Subsystem (RCS) will be used for stabilizing this tumbling asteroid and spacecraft combination. The RCS uses hypergolic bipropellant, comprising of monomethylhydrazine and nitrogen tetroxide with a gaseous pressured nitrogen. The RCS includes four pods of four thrusters as shown in Fig. 3(b). Each thruster has a maximum thrust output of 200 N and the fuel's specific impulse is 287 sec. The position, direction, and control influence matrix of the thrusters in the spacecraft frame $\mathcal{F}_S$ (see Fig. 4) are shown in Table 2, where an opposing pair of thrusters in a pod are represented by a single thruster capable of producing thrust between +200 N to −200 N. Note that during the capture and detumbling stage, the ARM-spacecraft's solar arrays will be folded back to facilitate the despinning process. In this paper, we develop attitude control strategies for despinning and three-axis stabilizing the tumbling asteroid and spacecraft combination using this RCS controller, in the presence of uncertain physical parameters, bounded disturbances, measurement errors, and actuator saturations. Note that we also presents specific design guidelines for the ARM spacecraft.

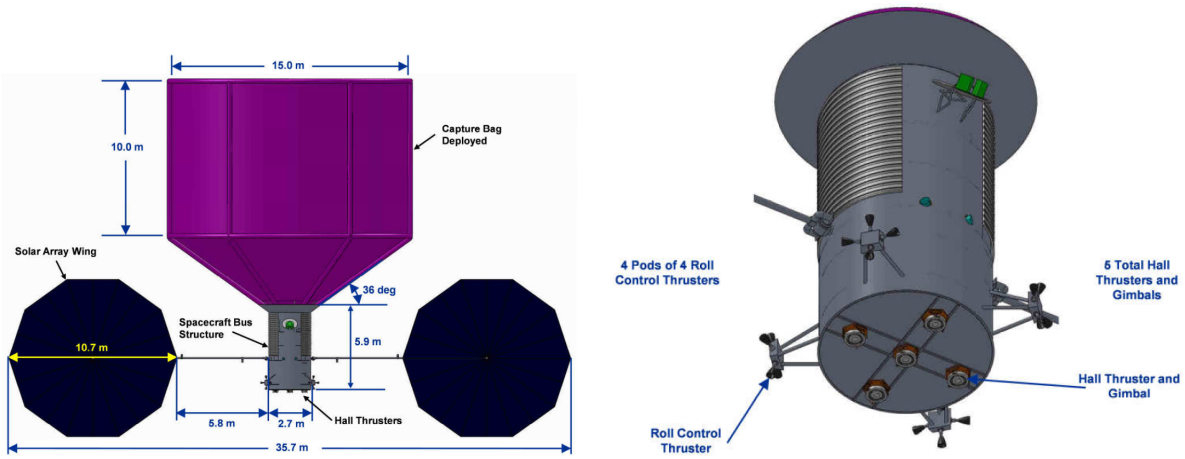

(a) (b)

Figure 3: (a) Conceptual design of the ARM spacecraft in the cruise configuration with the capture mechanism deployed, along with its dimensions (image credit: NASA[6]). (b) Bottom view of the conceptual ARM spacecraft with the five Hall thrusters and the four RCS thruster pods (image credit: NASA[6]).

B. Attitude Dynamics and Kinematics of the Asteroid and Spacecraft Combination

We assume that the asteroid and ARM spacecraft combination is a tumbling rigid body. Note that the slippage between the capture mechanism and the asteroid and the flexibility of the solar arrays are neglected in this paper. In this section, we present the attitude dynamics and kinematics equations that are used in this paper. We first present the dynamics equations of the rigid combination, then choose an appropriate attitude representation system, and finally describe the kinematics and dynamics of the rigid combination in the chosen attitude representation.

Table 2: RCS Thruster Position and Direction generated from Fig. 3

Thruster	Pod	Position of Thruster (m)	Direction of Thrust	Control Influence Matrix ($\boldsymbol{B}$)
u_1	P_1	$\boldsymbol{r}^{P_1/S_O} = 1.4\hat{s}_x + 5.9\hat{s}_z$	$\pm\hat{s}_y$	$\boldsymbol{B}(:,1) = (\boldsymbol{r}^{S_O/B_{CM}} + \boldsymbol{r}^{P_1/S_O}) \times (\hat{s}_y)$
u_2	P_1	$\boldsymbol{r}^{P_1/S_O} = 1.4\hat{s}_x + 5.9\hat{s}_z$	$\pm\hat{s}_z$	$\boldsymbol{B}(:,2) = (\boldsymbol{r}^{S_O/B_{CM}} + \boldsymbol{r}^{P_1/S_O}) \times (\hat{s}_z)$
u_3	P_2	$\boldsymbol{r}^{P_2/S_O} = 1.4\hat{s}_y + 5.9\hat{s}_z$	$\pm\hat{s}_x$	$\boldsymbol{B}(:,3) = (\boldsymbol{r}^{S_O/B_{CM}} + \boldsymbol{r}^{P_2/S_O}) \times (\hat{s}_x)$
u_4	P_2	$\boldsymbol{r}^{P_2/S_O} = 1.4\hat{s}_y + 5.9\hat{s}_z$	$\pm\hat{s}_z$	$\boldsymbol{B}(:,4) = (\boldsymbol{r}^{S_O/B_{CM}} + \boldsymbol{r}^{P_2/S_O}) \times (\hat{s}_z)$
u_5	P_3	$\boldsymbol{r}^{P_3/S_O} = -1.4\hat{s}_x + 5.9\hat{s}_z$	$\pm\hat{s}_y$	$\boldsymbol{B}(:,5) = (\boldsymbol{r}^{S_O/B_{CM}} + \boldsymbol{r}^{P_3/S_O}) \times (\hat{s}_y)$
u_6	P_3	$\boldsymbol{r}^{P_3/S_O} = -1.4\hat{s}_x + 5.9\hat{s}_z$	$\pm\hat{s}_z$	$\boldsymbol{B}(:,6) = (\boldsymbol{r}^{S_O/B_{CM}} + \boldsymbol{r}^{P_3/S_O}) \times (\hat{s}_z)$
u_7	P_4	$\boldsymbol{r}^{P_4/S_O} = -1.4\hat{s}_y + 5.9\hat{s}_z$	$\pm\hat{s}_x$	$\boldsymbol{B}(:,7) = (\boldsymbol{r}^{S_O/B_{CM}} + \boldsymbol{r}^{P_4/S_O}) \times (\hat{s}_x)$
u_8	P_4	$\boldsymbol{r}^{P_4/S_O} = -1.4\hat{s}_y + 5.9\hat{s}_z$	$\pm\hat{s}_z$	$\boldsymbol{B}(:,8) = (\boldsymbol{r}^{S_O/B_{CM}} + \boldsymbol{r}^{P_4/S_O}) \times (\hat{s}_z)$

The center of mass of the asteroid and spacecraft combination (B_{CM}) is the origin of the body fixed frame $\mathcal{F}_B$, as shown in Fig. 4. Let S_O, which is the base of the ARM-spacecraft's body, be the origin of the spacecraft frame $\mathcal{F}_S$ as shown in Fig. 4. We assume that attitude orientation of $\mathcal{F}_B$ with respect to $\mathcal{F}_I$ is the same as that of $\mathcal{F}_S$ with respect to $\mathcal{F}_I$, i.e., the rotation matrix from $\mathcal{F}_S$ to $\mathcal{F}_B$ is an identity matrix. Let $\boldsymbol{r}^{S_O/B_{CM}}$ denote the vector from B_{CM} to S_O.

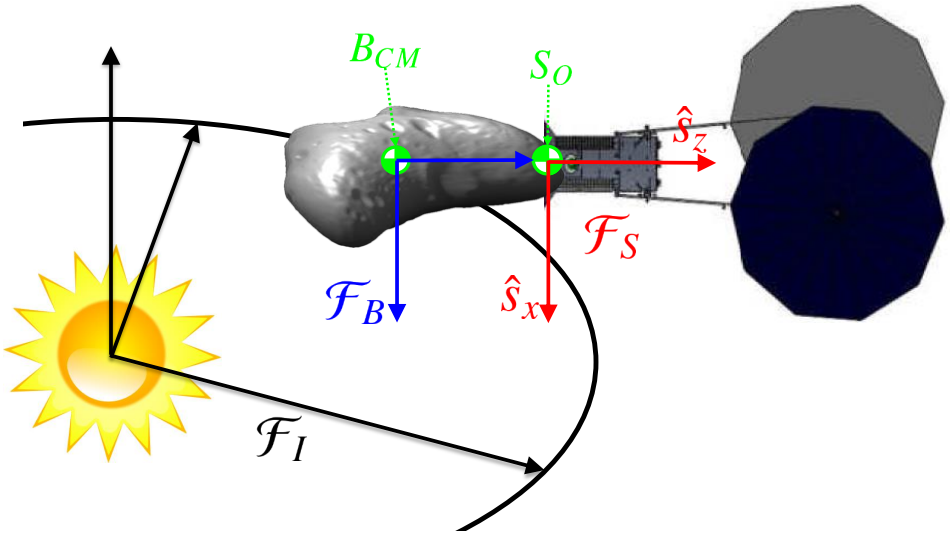

Figure 4: Reference Frames: the inertial frame $\mathcal{F}_I$, the body fixed frame $\mathcal{F}_B$, and the spacecraft frame $\mathcal{F}_S$.

1. *Dynamics Equation*

Let $\boldsymbol{J}_{\text{ast}}^{B_{CM}}$ be the unknown, constant, positive-definite inertia tensor of the asteroid at B_{CM} and expressed in $\mathcal{F}_B$. Let $\boldsymbol{J}_{\text{sc}}^{S_{CM}}$ be the known, constant, positive-definite inertia tensor of the ARM spacecraft at the center of mass of the ARM spacecraft (S_{CM}) and expressed in $\mathcal{F}_S$. The combined inertia tensor of the asteroid and spacecraft combination at B_{CM} and expressed in $\mathcal{F}_B$ is determined using the parallel axis theorem to be:

$$\boldsymbol{J}_{\text{tot}}^{B_{CM}} = \boldsymbol{J}_{\text{ast}}^{B_{CM}} + \boldsymbol{J}_{\text{sc}}^{S_{CM}} + m_{\text{sc}} \left[\left(\boldsymbol{r}^{S_{CM}/B_{CM}}\right)^T \left(\boldsymbol{r}^{S_{CM}/B_{CM}}\right) \mathbf{I} - \left(\boldsymbol{r}^{S_{CM}/B_{CM}}\right) \left(\boldsymbol{r}^{S_{CM}/B_{CM}}\right)^T \right], \quad (1)$$

where $\boldsymbol{r}^{S_{CM}/B_{CM}} = \boldsymbol{r}^{S_{CM}/S_O} + \boldsymbol{r}^{S_O/B_{CM}}$, $\boldsymbol{r}^{S_{CM}/S_O}$ is the known vector from S_O to S_{CM}, m_{sc} is the mass of the ARM spacecraft, and the rotation matrix from the spacecraft frame to the body frame is an identity matrix.

Let $\boldsymbol{\omega} \in \mathbb{R}^3$ be the angular velocity of the asteroid and spacecraft combination in the body fixed frame $\mathcal{F}_B$ with respect to the inertial frame $\mathcal{F}_I$ and expressed in the frame $\mathcal{F}_B$. In Table 2, the thrust outputs of the eight thrusters $\boldsymbol{u} \in \mathbb{R}^8$ and the control influence matrix for the thrusters $\boldsymbol{B} \in \mathbb{R}^{3\times 8}$ are shown. Let $\boldsymbol{d}_{\text{ext}} \in \mathbb{R}^3$ denote the external disturbance torques on the system. The dynamics of the rigid asteroid and spacecraft combination is modeled as:[47,48]

$$\boldsymbol{J}_{\text{tot}}^{B_{CM}} \dot{\boldsymbol{\omega}} = \left(\boldsymbol{J}_{\text{tot}}^{B_{CM}} \boldsymbol{\omega} \right) \times \boldsymbol{\omega} + \boldsymbol{B}\boldsymbol{u} + \boldsymbol{d}_{\text{ext}} \,. \tag{2}$$

2. *Attitude Representation*

We now choose an appropriate attitude representation for this problem. The attitude orientation of the body frame $\mathcal{F}_B$ with respect to the inertial frame $\mathcal{F}_I$ should be represented using an attitude representation that is global, i.e., can represent any possible orientation; and is preferably unique, i.e., there is only one representation for every possible orientation. Table 3, adapted from Ref. 49, lists the properties of various attitude representations.

Table 3: Properties of Attitude Representations (adapted from Ref. 49)

Attitude Representation	Range, Transformation	Global?	Unique?
Euler Angles	$\phi,\, \theta,\, \psi \in [-\pi, \pi]$	No ($\theta = \pm\pi/2$)	No
Euler Axis of Rotation and Angle	$\boldsymbol{e} \in \mathbb{S}^2,\ \Phi \in [-\pi, \pi]$	Yes	No ($\boldsymbol{e}^S = -\boldsymbol{e}$, $\Phi^S = 2\pi - \Phi$)
Quaternions	$\boldsymbol{\beta} \in \mathbb{S}^3$, $\beta_i = e_i \sin\frac{\Phi}{2}, i \in \{1,2,3\}$, $\beta_4 = \cos\frac{\Phi}{2}$	Yes	No ($\boldsymbol{\beta}^S = -\boldsymbol{\beta}$)
Classical Rodrigues Parameters	$\boldsymbol{\sigma} \in \mathbb{R}^3$, $\boldsymbol{\sigma} = \boldsymbol{e}\tan\frac{\Phi}{2}$	No (Singularity at $\Phi = \pm\pi$)	Yes
Modified Rodrigues Parameters (MRP)	$\boldsymbol{q} \in \mathbb{R}^3$, $\boldsymbol{q} = \boldsymbol{e}\tan\frac{\Phi}{4}$	No (Singularity at $\Phi = 2\pi$)	No ($\boldsymbol{q}^S = -\boldsymbol{e}\tan\frac{2\pi-\Phi}{4}$)
Rotation Matrix SO(3)	$\boldsymbol{R} \in \mathbb{R}^{3\times 3}$, $\boldsymbol{R}\boldsymbol{R}^T = \mathbf{I}$, $\boldsymbol{R}^T\boldsymbol{R} = \mathbf{I}$, $\det(\boldsymbol{R}) = 1$	Yes	Yes

In Table 3, $(\cdot)^S$ denotes the shadow point representation of the same attitude. Note that classical Rodrigues parameters are unique because:[50]

$$\boldsymbol{\sigma}^S = -\boldsymbol{e}\tan\frac{2\pi - \Phi}{2} = \boldsymbol{e}\tan\frac{\Phi}{2} = \boldsymbol{\sigma} \,. \tag{3}$$

Note that $\boldsymbol{e} \in \mathbb{S}^2$ and $\Phi \in [-\pi, \pi]$ captures all possible orientations. If we restrict the Euler angle range to be within $\Phi \in [-\pi, \pi]$, then MRP is global in its representation of attitude as there is no singularity in this range and the ℓ_2-norm of MRP is upper-bounded by 1, i.e., $\|\boldsymbol{q}\|_2 \leq 1$. Therefore MRP becomes both global and unique with this constraint. In this paper, we use both quaternions and MRP (without the constraint) for attitude representation, depending on the ease of designing control laws.

3. *Euler–Lagrangian Formulation*

We now develop a combined representation of the kinematics and dynamics equations of the asteroid and spacecraft combination using MRP. The kinematics of the rigid asteroid and spacecraft combination using

quaternions is given by:[47,48]

$$\dot{\boldsymbol{\beta}}_v = \frac{1}{2}(\beta_4\boldsymbol{\omega} + \boldsymbol{\beta}_v \times \boldsymbol{\omega})\,, \qquad \dot{\beta}_4 = -\frac{1}{2}\boldsymbol{\beta}_v^T\boldsymbol{\omega}\,, \tag{4}$$

where $\boldsymbol{\beta}_v = [\beta_1,\, \beta_2,\, \beta_3] \in \mathbb{R}^3$ and $\boldsymbol{\beta} = [\boldsymbol{\beta}_v,\, \beta_4] \in \mathbb{S}^3$. The corresponding kinematics equation of a rigid body using MRP is given by:[51]

$$\begin{aligned} &\dot{\boldsymbol{q}} = \boldsymbol{Z}(\boldsymbol{q})\boldsymbol{\omega}\,, \\ \text{where}\quad &\boldsymbol{Z}(\boldsymbol{q}) = \frac{1}{2}\left[\mathbf{I}\left(\frac{1-\boldsymbol{q}^T\boldsymbol{q}}{2}\right) + \boldsymbol{q}\boldsymbol{q}^T + \boldsymbol{S}(\boldsymbol{q})\right]\,, \quad \boldsymbol{S}(\boldsymbol{q}) = \begin{bmatrix} 0 & -q_3 & q_2 \\ q_3 & 0 & -q_1 \\ -q_2 & q_1 & 0 \end{bmatrix}. \end{aligned} \tag{5}$$

The combined kinematics and dynamics of the rigid asteroid and spacecraft combination using MRP is given by:[51,52]

$$\begin{aligned} &\boldsymbol{M}(\boldsymbol{q})\ddot{\boldsymbol{q}} + \boldsymbol{C}(\boldsymbol{q},\dot{\boldsymbol{q}})\dot{\boldsymbol{q}} = \boldsymbol{\tau}_c + \boldsymbol{\tau}_{\text{ext}}\,, \\ \text{where}\quad &\boldsymbol{M}(\boldsymbol{q}) = \boldsymbol{Z}^{-T}(\boldsymbol{q})\boldsymbol{J}_{\text{tot}}^{B_{CM}}\boldsymbol{Z}^{-1}(\boldsymbol{q})\,, \\ &\boldsymbol{C}(\boldsymbol{q},\dot{\boldsymbol{q}}) = -\boldsymbol{Z}^{-T}\boldsymbol{J}_{\text{tot}}^{B_{CM}}\boldsymbol{Z}^{-1}\dot{\boldsymbol{Z}}\boldsymbol{Z}^{-1} - \boldsymbol{Z}^{-T}\boldsymbol{S}(\boldsymbol{J}_{\text{tot}}^{B_{CM}}\boldsymbol{Z}^{-1}\dot{\boldsymbol{q}})\boldsymbol{Z}^{-1}\,, \\ &\boldsymbol{\tau}_c = \boldsymbol{Z}^{-T}(\boldsymbol{q})\boldsymbol{B}\boldsymbol{u}\,, \qquad \boldsymbol{\tau}_{\text{ext}} = \boldsymbol{Z}^{-T}(\boldsymbol{q})\boldsymbol{d}_{\text{ext}}\,. \end{aligned} \tag{6}$$

Equation (6) is the Euler–Lagrangian (EL) formulation of the attitude kinematics and dynamics of a rigid asteroid and spacecraft combination. Note that $\dot{\boldsymbol{M}}(\boldsymbol{q}) - 2\boldsymbol{C}(\boldsymbol{q},\dot{\boldsymbol{q}})$ in Eq. (6) is a skew-symmetric matrix, but both $\boldsymbol{M}(\boldsymbol{q})$ and $\boldsymbol{C}(\boldsymbol{q},\dot{\boldsymbol{q}})$ matrices are unknown as they depend on the unknown inertia tensor $\boldsymbol{J}_{\text{tot}}^{B_{CM}}$. In the next section, we state the control problem statement of this paper.

C. Problem Statement: Attitude Control and Stabilization of the Asteroid and Spacecraft Combination

The main objective of this paper is to develop attitude control strategies for stabilizing the tumbling asteroid and spacecraft combination. The salient features of this attitude control problem are as follows:

1. The asteroid and ARM spacecraft combination is tumbling. The tumbling rate can be nonuniform due to the cross-terms in the moment of inertia tensor.

2. The asteroid's inertia tensor, mass, center of mass, and center of gravity have large uncertainties (approximately 10% of the nominal value).

3. The asteroid is non-collaborative; i.e., no actuators are placed on the asteroid. All actuators are onboard the ARM spacecraft.

The attitude control objective is to detumble and three-axis stabilize the asteroid and spacecraft combination, which is formulated as an EL system using the MRP representation in Eq. (6). Let the MRP $\boldsymbol{q}_{\text{final}}$ (or the quaternion $\boldsymbol{\beta}_{\text{final}}$) be the desired attitude orientation of the stabilized EL system. The control objective is to stabilize the EL system, in the presence of uncertain physical parameters, bounded disturbances, measurement errors, and actuator saturations, such that for some $\varepsilon_{\text{trans}} > 0$, $\varepsilon_{\text{ss}} > 0$, and $T > 0$:

$$\|\boldsymbol{\omega}(t)\|_2 \le \varepsilon_{\text{trans}}, \qquad \forall t \in \mathbb{R}\,, \tag{7}$$

$$\|\boldsymbol{q}(t) - \boldsymbol{q}_{\text{final}}\|_2 \le \varepsilon_{\text{ss}}, \qquad \forall t > T\,. \tag{8}$$

The transient error bound $\varepsilon_{\text{trans}}$ is imposed on the angular velocity $\boldsymbol{\omega}(t)$ in Eq. (7) in order to ensure that the system is always within the technological capability of the sensors and actuators onboard the ARM spacecraft. It is desired that after time $T \in \mathbb{R}$, the asteroid and spacecraft combination should be oriented in the desired attitude orientation, represented by the MRP $\boldsymbol{q}_{\text{final}}$, as shown in the steady-state condition

(8). Note that if the system has to hold its attitude within the given steady-state error bound ε_{ss}, then the desired angular velocity $\boldsymbol{\omega}_{\text{final}}$ of the stabilized system should be sufficiently close to $\mathbf{0}$ rpm.

Note that a control law that yields global exponential convergence in the absence of disturbance is preferred for this control problem because it is possible to ensure that the error in the EL system's trajectory $\|\boldsymbol{q}(t) - \boldsymbol{q}_{\text{final}}\|_2$, in the presence of bounded disturbances and errors, is ultimately bounded by the given bound ε_{ss}.[53] If a control law that only yields global asymptotic convergence without any disturbance (e.g., proportional-derivative control law for Eq. (6)) is used then the error in the EL system's trajectory, in the presence of bounded disturbances and errors, may not be bounded.[53] Fortunately, in case of the proportional-derivative control law, shown in Fig. 6, the realistic disturbances and errors are benign and the error in the EL system's trajectory is ultimately bounded by the given steady-state error bound ε_{ss}.

III. Fundamental Limit on Control Laws for Attitude Control and Stabilization

Let us divide the attitude control laws into two classes: (i) control laws that use the dynamics equation of the system (2) in the control law equation and (ii) control laws that do not use the dynamics of the system in the control law equation. The objective of this section is to show that control laws belonging to class (i) encounter a fundamental limitation due to large modeling uncertainties. We show that the resultant disturbance torque for such control laws is comparable to the maximum control torque of the conceptual ARM spacecraft in the presence of large modeling uncertainties. In contrast, control laws belonging to class (ii) experience a much smaller resultant disturbance torque in the presence of large modeling uncertainties.

Let us first consider the control laws belonging to class (i), i.e., control laws that use the dynamics equation of the system (2) in the control law equation and consequently terms like $\boldsymbol{M}(\boldsymbol{q})$, $\boldsymbol{C}(\boldsymbol{q},\dot{\boldsymbol{q}})$, $\boldsymbol{J}_{\text{tot}}^{B_{CM}}$ enter the control law equation. Here we study the effect of modeling uncertainties in $\boldsymbol{J}_{\text{ast}}^{B_{CM}}$ and $\boldsymbol{r}^{S_O/B_{CM}}$, measurement errors in $\boldsymbol{\omega}$, and actuator errors in $\boldsymbol{u}$ on the dynamics of the asteroid and spacecraft combination (2). Let $\boldsymbol{J}_{\text{ast}}^{B_{CM}} = \hat{\boldsymbol{J}}_{\text{ast}}^{B_{CM}} + \Delta\boldsymbol{J}_{\text{ast}}^{B_{CM}}$, where $\hat{\boldsymbol{J}}_{\text{ast}}^{B_{CM}}$ is the estimated inertia tensor of the asteroid and $\Delta\boldsymbol{J}_{\text{ast}}^{B_{CM}}$ is the modeling error. Similarly, $\boldsymbol{r}^{S_O/B_{CM}} = \hat{\boldsymbol{r}}^{S_O/B_{CM}} + \Delta\boldsymbol{r}^{S_O/B_{CM}}$, $\boldsymbol{\omega} = \hat{\boldsymbol{\omega}} + \Delta\boldsymbol{\omega}$ and $\boldsymbol{u} = \hat{\boldsymbol{u}} + \Delta\boldsymbol{u}$. The effect of these modeling uncertainties on $\boldsymbol{J}_{\text{tot}}^{B_{CM}}$ is given by:

$$
\begin{aligned}
\boldsymbol{J}_{\text{tot}}^{B_{CM}} &= \hat{\boldsymbol{J}}_{\text{ast}}^{B_{CM}} + \Delta\boldsymbol{J}_{\text{ast}}^{B_{CM}} + \boldsymbol{J}_{\text{sc}}^{S_{CM}} \\
&\quad + m_{\text{sc}} \begin{bmatrix} \left(\boldsymbol{r}^{S_{CM}/S_O} + \hat{\boldsymbol{r}}^{S_O/B_{CM}} + \Delta\boldsymbol{r}^{S_O/B_{CM}}\right)^T \left(\boldsymbol{r}^{S_{CM}/S_O} + \hat{\boldsymbol{r}}^{S_O/B_{CM}} + \Delta\boldsymbol{r}^{S_O/B_{CM}}\right)\mathbf{I} \\ -\left(\boldsymbol{r}^{S_{CM}/S_O} + \hat{\boldsymbol{r}}^{S_O/B_{CM}} + \Delta\boldsymbol{r}^{S_O/B_{CM}}\right)\left(\boldsymbol{r}^{S_{CM}/S_O} + \hat{\boldsymbol{r}}^{S_O/B_{CM}} + \Delta\boldsymbol{r}^{S_O/B_{CM}}\right)^T \end{bmatrix}, \\
\boldsymbol{J}_{\text{tot}}^{B_{CM}} &= \underbrace{\hat{\boldsymbol{J}}_{\text{ast}}^{B_{CM}} + \boldsymbol{J}_{\text{sc}}^{S_{CM}} + m_{\text{sc}} \begin{bmatrix} \left(\boldsymbol{r}^{S_{CM}/S_O} + \hat{\boldsymbol{r}}^{S_O/B_{CM}}\right)^T \left(\boldsymbol{r}^{S_{CM}/S_O} + \hat{\boldsymbol{r}}^{S_O/B_{CM}}\right)\mathbf{I} \\ -\left(\boldsymbol{r}^{S_{CM}/S_O} + \hat{\boldsymbol{r}}^{S_O/B_{CM}}\right)\left(\boldsymbol{r}^{S_{CM}/S_O} + \hat{\boldsymbol{r}}^{S_O/B_{CM}}\right)^T \end{bmatrix}}_{\hat{\boldsymbol{J}}_{\text{tot}}^{B_{CM}}} \\
&\quad + \underbrace{\Delta\boldsymbol{J}_{\text{ast}}^{B_{CM}} + m_{\text{sc}} \begin{bmatrix} 2\left(\Delta\boldsymbol{r}^{S_O/B_{CM}}\right)^T \left(\boldsymbol{r}^{S_{CM}/S_O} + \hat{\boldsymbol{r}}^{S_O/B_{CM}}\right)\mathbf{I} \\ -\left(\Delta\boldsymbol{r}^{S_O/B_{CM}}\right)\left(\boldsymbol{r}^{S_{CM}/S_O} + \hat{\boldsymbol{r}}^{S_O/B_{CM}}\right)^T \\ -\left(\boldsymbol{r}^{S_{CM}/S_O} + \hat{\boldsymbol{r}}^{S_O/B_{CM}}\right)\left(\Delta\boldsymbol{r}^{S_O/B_{CM}}\right)^T \end{bmatrix}}_{\Delta\boldsymbol{J}_{\text{tot}}^{B_{CM}}}.
\end{aligned} \tag{9}
$$

Hence we get $\boldsymbol{J}_{\text{tot}}^{B_{CM}} = \hat{\boldsymbol{J}}_{\text{tot}}^{B_{CM}} + \Delta\boldsymbol{J}_{\text{tot}}^{B_{CM}}$. Note that we have neglected the second order error terms. Similarly, the control influence matrix from Table 2 can also be decomposed into $\boldsymbol{B} = \hat{\boldsymbol{B}} + \Delta\boldsymbol{B}$. Simplifying the dynamics of the asteroid and spacecraft combination (2) gives:

$$
\begin{aligned}
(\hat{\boldsymbol{J}}_{\text{tot}}^{B_{CM}} + \Delta\boldsymbol{J}_{\text{tot}}^{B_{CM}})(\dot{\hat{\boldsymbol{\omega}}} + \Delta\dot{\boldsymbol{\omega}}) &= \Big((\hat{\boldsymbol{J}}_{\text{tot}}^{B_{CM}} + \Delta\boldsymbol{J}_{\text{tot}}^{B_{CM}})(\hat{\boldsymbol{\omega}} + \Delta\boldsymbol{\omega})\Big) \times (\hat{\boldsymbol{\omega}} + \Delta\boldsymbol{\omega}) \\
&\quad + (\hat{\boldsymbol{B}} + \Delta\boldsymbol{B})(\hat{\boldsymbol{u}} + \Delta\boldsymbol{u}) + \boldsymbol{d}_{\text{ext}}\,, \\
\hat{\boldsymbol{J}}_{\text{tot}}^{B_{CM}}\dot{\hat{\boldsymbol{\omega}}} + \Delta\boldsymbol{J}_{\text{tot}}^{B_{CM}}\dot{\hat{\boldsymbol{\omega}}} + \hat{\boldsymbol{J}}_{\text{tot}}^{B_{CM}}\Delta\dot{\boldsymbol{\omega}} &= \Big(\hat{\boldsymbol{J}}_{\text{tot}}^{B_{CM}}\hat{\boldsymbol{\omega}} + \Delta\boldsymbol{J}_{\text{tot}}^{B_{CM}}\hat{\boldsymbol{\omega}} + \hat{\boldsymbol{J}}_{\text{tot}}^{B_{CM}}\Delta\boldsymbol{\omega} + \Delta\boldsymbol{J}_{\text{tot}}^{B_{CM}}\Delta\boldsymbol{\omega}\Big) \times (\hat{\boldsymbol{\omega}} + \Delta\boldsymbol{\omega}) \\
&\quad + (\hat{\boldsymbol{B}}\hat{\boldsymbol{u}} + \Delta\boldsymbol{B}\hat{\boldsymbol{u}} + \hat{\boldsymbol{B}}\Delta\boldsymbol{u}) + \boldsymbol{d}_{\text{ext}}\,,
\end{aligned}
$$

$$
\hat{\boldsymbol{J}}_{\text{tot}}^{B_{CM}}\dot{\hat{\boldsymbol{\omega}}} = \hat{\boldsymbol{J}}_{\text{tot}}^{B_{CM}}\hat{\boldsymbol{\omega}} \times \hat{\boldsymbol{\omega}} + \hat{\boldsymbol{B}}\hat{\boldsymbol{u}} + \underbrace{\begin{bmatrix} \Delta\boldsymbol{J}_{\text{tot}}^{B_{CM}}\hat{\boldsymbol{\omega}} \times \hat{\boldsymbol{\omega}} + \Big(\hat{\boldsymbol{J}}_{\text{tot}}^{B_{CM}} + \Delta\boldsymbol{J}_{\text{tot}}^{B_{CM}}\Big)\Delta\boldsymbol{\omega} \times \hat{\boldsymbol{\omega}} \\ + \Big(\hat{\boldsymbol{J}}_{\text{tot}}^{B_{CM}} + \Delta\boldsymbol{J}_{\text{tot}}^{B_{CM}}\Big)\hat{\boldsymbol{\omega}} \times \Delta\boldsymbol{\omega} \\ + \Delta\boldsymbol{B}\hat{\boldsymbol{u}} + \hat{\boldsymbol{B}}\Delta\boldsymbol{u} - \Delta\boldsymbol{J}_{\text{tot}}^{B_{CM}}\dot{\hat{\boldsymbol{\omega}}} - \hat{\boldsymbol{J}}_{\text{tot}}^{B_{CM}}\Delta\dot{\boldsymbol{\omega}} + \boldsymbol{d}_{\text{ext}} \end{bmatrix}}_{\boldsymbol{d}_{\text{res}}}. \tag{10}
$$

Thus $\boldsymbol{d}_{\text{res}}$ in Eq. (10) is the resultant disturbance torque acting on the system due to these bounded disturbances, modeling uncertainties, measurement errors, and actuator errors. Each of the thrusters in Table 2 can produce a maximum thrust of magnitude $u_{\max}$. The maximum control torque that the conceptual ARM spacecraft can generate is given by $\boldsymbol{\tau}_{\max} = \boldsymbol{B}\mathbf{1}u_{\max}$, which is approximately $\|\boldsymbol{\tau}_{\max}\|_2 \approx 10^3$ Nm. For a valid control strategy to exist, the resultant disturbance torque $\boldsymbol{d}_{\text{res}}$ on the dynamics of the asteroid and spacecraft combination should be less than the maximum control torque of the conceptual ARM spacecraft $\boldsymbol{\tau}_{\max}$, i.e., $\|\boldsymbol{d}_{\text{res}}\|_2 < \|\boldsymbol{\tau}_{\max}\|_2$.

Table 4: Magnitude of some of the disturbance terms in the resultant disturbance torques

Disturbance term	Magnitude (ℓ_2-norm)	Disturbance term present in $\boldsymbol{d}_{\text{res}}$ in Eq. (10)	Disturbance term present in $\tilde{\boldsymbol{d}}_{\text{res}}$ in Eq. (11)
$\Delta\boldsymbol{J}_{\text{tot}}^{B_{CM}}\hat{\boldsymbol{\omega}} \times \hat{\boldsymbol{\omega}}$	372.8 Nm	✓	✗
$\hat{\boldsymbol{J}}_{\text{tot}}^{B_{CM}}\Delta\boldsymbol{\omega} \times \hat{\boldsymbol{\omega}}$	7.8 Nm	✓	✓
$\Delta\boldsymbol{J}_{\text{tot}}^{B_{CM}}\Delta\boldsymbol{\omega} \times \hat{\boldsymbol{\omega}}$	6.3 Nm	✓	✓
$\hat{\boldsymbol{J}}_{\text{tot}}^{B_{CM}}\hat{\boldsymbol{\omega}} \times \Delta\boldsymbol{\omega}$	10.1 Nm	✓	✓
$\Delta\boldsymbol{J}_{\text{tot}}^{B_{CM}}\hat{\boldsymbol{\omega}} \times \Delta\boldsymbol{\omega}$	7.3 Nm	✓	✓

$$
\text{where } \boldsymbol{J}_{\text{tot}}^{B_{CM}} = 10^6 \times \begin{bmatrix} 1.2652 & 0.4397 & 0.0015 \\ 0.4397 & 3.8688 & 0.0002 \\ 0.0015 & 0.0002 & 3.5440 \end{bmatrix} \text{ kg m}^2\,, \quad \hat{\boldsymbol{J}}_{\text{tot}}^{B_{CM}} = 10^6 \times \begin{bmatrix} 1 & 0 & 0 \\ 0 & 3 & 0 \\ 0 & 0 & 3 \end{bmatrix} \text{ kg m}^2\,,
$$

$$
\boldsymbol{\omega} = [\ 0.01 \quad 0.02 \quad 0.03\ ] \text{ rad sec}^{-1}\,, \quad \hat{\boldsymbol{\omega}} = [\ 0.010 \quad 0.020 \quad 0.0299\ ] \text{ rad sec}^{-1}\,,
$$

$$
\|\Delta\boldsymbol{J}_{\text{tot}}^{B_{CM}}\|_2 \approx 10^6 \text{ kg m}^2\,, \quad \Delta\boldsymbol{\omega} = 10^{-4} \times [\ -0.44 \quad 0.09 \quad 0.91\ ] \text{ rad sec}^{-1}\,.
$$

Table 4 shows the magnitude of some of the disturbance terms in $\boldsymbol{d}_{\text{res}}$ (10) for the given example. Note that the magnitude of the disturbance term $(\Delta\boldsymbol{J}_{\text{tot}}^{B_{CM}}\hat{\boldsymbol{\omega}} \times \hat{\boldsymbol{\omega}})$ is significantly larger than the magnitude of other disturbance terms. Moreover a large amount of control effort (approximately 40% of the conceptual ARM-spacecraft's maximum control torque) is needed to counter this disturbance term. In certain cases when $\|\Delta\boldsymbol{J}_{\text{tot}}^{B_{CM}}\|_2 \approx 10^7$ kg m^2 and $\|\Delta\boldsymbol{J}_{\text{tot}}^{B_{CM}}\hat{\boldsymbol{\omega}} \times \hat{\boldsymbol{\omega}}\|_2 \approx 10^3$, it is seen that $\|\boldsymbol{d}_{\text{res}}\|_2 > \|\boldsymbol{\tau}_{\max}\|_2$ and the conceptual ARM spacecraft does not have sufficient control torque to stabilize the system. Hence this disturbance term, which arises from modeling uncertainties, puts a fundamental limit on the use of control laws belonging to class (i) for this control problem.

Let us now consider the control laws belonging to class (ii), i.e., control laws that do not use the dynamics of the system in the control law equation. Simplifying the dynamics of the asteroid and spacecraft combination (2) for this case gives:

$$(\hat{\boldsymbol{J}}_{\text{tot}}^{B_{CM}}+\Delta\boldsymbol{J}_{\text{tot}}^{B_{CM}})\dot{\hat{\boldsymbol{\omega}}}=(\hat{\boldsymbol{J}}_{\text{tot}}^{B_{CM}}+\Delta\boldsymbol{J}_{\text{tot}}^{B_{CM}})\hat{\boldsymbol{\omega}}\times\hat{\boldsymbol{\omega}}+\hat{\boldsymbol{B}}\hat{\boldsymbol{u}}+\underbrace{\begin{bmatrix}\left(\hat{\boldsymbol{J}}_{\text{tot}}^{B_{CM}}+\Delta\boldsymbol{J}_{\text{tot}}^{B_{CM}}\right)\Delta\boldsymbol{\omega}\times\hat{\boldsymbol{\omega}}\\+\left(\hat{\boldsymbol{J}}_{\text{tot}}^{B_{CM}}+\Delta\boldsymbol{J}_{\text{tot}}^{B_{CM}}\right)\hat{\boldsymbol{\omega}}\times\Delta\boldsymbol{\omega}\\+\Delta\boldsymbol{B}\hat{\boldsymbol{u}}+\hat{\boldsymbol{B}}\Delta\boldsymbol{u}-\hat{\boldsymbol{J}}_{\text{tot}}^{B_{CM}}\Delta\dot{\boldsymbol{\omega}}+\boldsymbol{d}_{\text{ext}}\end{bmatrix}}_{\tilde{\boldsymbol{d}}_{\text{res}}}. \quad (11)$$

In this case, the significant disturbance term $(\Delta\boldsymbol{J}_{\text{tot}}^{B_{CM}}\hat{\boldsymbol{\omega}}\times\hat{\boldsymbol{\omega}})$ does not enter the resultant disturbance torque $\tilde{\boldsymbol{d}}_{\text{res}}$ in Eq. (11). Hence the magnitude of the resultant disturbance torque $\tilde{\boldsymbol{d}}_{\text{res}}$ in Eq. (11) is much smaller than $\boldsymbol{d}_{\text{res}}$ in Eq. (10). For a valid control strategy to exist, we need to ensure that $\|\tilde{\boldsymbol{d}}_{\text{res}}\|_2 < \|\boldsymbol{\tau}_{\max}\|_2$. The advantage of the smaller resultant disturbance torque for control laws belonging to class (ii) is shown in the numerical simulations.

IV. Control Laws for Attitude Control and Stabilization with Uncertainty

In this section, we present three attitude control laws for despinning and three-axis stabilizing the asteroid and spacecraft combination. The first control law, discussed in Section IV.A, is the robust nonlinear tracking control law that globally exponentially stabilizes the system. In Section IV.B, the adaptive nonlinear tracking control law is presented, which also globally exponentially stabilizes the system. The third control strategy, discussed in Section IV.C, is to first globally-exponentially despin the system using a derivative (rate damping) linear control law and then globally-asymptotically stabilize the system in the desired attitude orientation using the simple proportional-derivative linear control law. Unlike the previous two control laws, the third control strategy does not use the dynamics of the system in the control law equation.

A. Robust Nonlinear Tracking Control Law

The EL formulation (6), discussed in Section II.B, does not account for the modeling uncertainties and measurement errors. The modified EL formulation, in the presence of the uncertainties and errors discussed in Section III, is given by:

$$\begin{aligned}&\hat{\boldsymbol{M}}(\hat{\boldsymbol{q}})\ddot{\hat{\boldsymbol{q}}}+\hat{\boldsymbol{C}}(\hat{\boldsymbol{q}},\dot{\hat{\boldsymbol{q}}})\dot{\hat{\boldsymbol{q}}}=\hat{\boldsymbol{\tau}}_c+\boldsymbol{\tau}_{\text{res}}\,, \quad (12)\\ \text{where}\quad &\hat{\boldsymbol{M}}(\hat{\boldsymbol{q}})=\boldsymbol{Z}^{-T}(\hat{\boldsymbol{q}})\hat{\boldsymbol{J}}_{\text{tot}}^{B_{CM}}\boldsymbol{Z}^{-1}(\hat{\boldsymbol{q}})\,,\qquad \hat{\boldsymbol{\tau}}_c=\boldsymbol{Z}^{-T}(\hat{\boldsymbol{q}})\hat{\boldsymbol{B}}\hat{\boldsymbol{u}}\,,\qquad \boldsymbol{\tau}_{\text{res}}=\boldsymbol{Z}^{-T}(\hat{\boldsymbol{q}})\boldsymbol{d}_{\text{res}}\,,\\ &\hat{\boldsymbol{C}}(\hat{\boldsymbol{q}},\dot{\hat{\boldsymbol{q}}})=-\boldsymbol{Z}^{-T}(\hat{\boldsymbol{q}})\hat{\boldsymbol{J}}_{\text{tot}}^{B_{CM}}\boldsymbol{Z}^{-1}(\hat{\boldsymbol{q}})\dot{\boldsymbol{Z}}(\hat{\boldsymbol{q}})\boldsymbol{Z}^{-1}(\hat{\boldsymbol{q}})-\boldsymbol{Z}^{-T}(\hat{\boldsymbol{q}})\,\boldsymbol{S}\left(\hat{\boldsymbol{J}}_{\text{tot}}^{B_{CM}}\boldsymbol{Z}^{-1}(\hat{\boldsymbol{q}})\dot{\hat{\boldsymbol{q}}}\right)\boldsymbol{Z}^{-1}(\hat{\boldsymbol{q}})\,.\end{aligned}$$

Here $\boldsymbol{d}_{\text{res}}$ is the resultant disturbance torque defined in Eq. (10). The following robust nonlinear tracking control law for the modified EL system (12) guarantees global exponential stability:[51]

$$\begin{aligned}&\hat{\boldsymbol{\tau}}_c=\hat{\boldsymbol{M}}(\hat{\boldsymbol{q}})\ddot{\boldsymbol{q}}_r+\hat{\boldsymbol{C}}(\hat{\boldsymbol{q}},\dot{\hat{\boldsymbol{q}}})\dot{\boldsymbol{q}}_r-\boldsymbol{K}_r\boldsymbol{s}\,, \quad (13)\\ \text{where}\quad &\dot{\boldsymbol{q}}_r=\dot{\boldsymbol{q}}_d(t)+\boldsymbol{\Lambda}_r(\boldsymbol{q}_d(t)-\hat{\boldsymbol{q}})\,,\qquad \boldsymbol{s}=\dot{\hat{\boldsymbol{q}}}-\dot{\boldsymbol{q}}_r\,,\end{aligned}$$

where the positive-definite matrix $\boldsymbol{K}_r\in\mathbb{R}^{3\times3}$ is the feedback gain, $\boldsymbol{\Lambda}_r\in\mathbb{R}^{3\times3}$ is a positive-definite matrix and $\boldsymbol{q}_d(t)$ is the time-varying desired (reference) trajectory.

The stability proof of this control law, given in Ref. 51, states that all system trajectories converge exponentially fast to a single trajectory regardless of initial conditions with a rate given by:

$$\lambda_{\text{conv,robust}}=\frac{\lambda_{\min}(\boldsymbol{K}_r)}{\lambda_{\max}(\hat{\boldsymbol{M}}(\hat{\boldsymbol{q}}))}\,, \quad (14)$$

where $\lambda_{\min}(\boldsymbol{K}_r)$ is the smallest eigenvalue of the matrix $\boldsymbol{K}_r$ and $\lambda_{\max}(\hat{\boldsymbol{M}}(\hat{\boldsymbol{q}}))$ is the largest eigenvalue of the positive definite matrix $\hat{\boldsymbol{M}}(\hat{\boldsymbol{q}})$. Let $\delta\boldsymbol{s}$ represent an infinitesimal change in the composite variable $\boldsymbol{s}$ defined in Eq. (13) and let $\Theta^T\Theta=\hat{\boldsymbol{M}}(\hat{\boldsymbol{q}})$. Let $P_1(t)$ be a solution of the contracting system without any disturbance and let $P_2(t)$ denote a trajectory of the system in the presence of disturbance $\boldsymbol{\tau}_{\text{res}}$, where $\Theta\boldsymbol{\tau}_{\text{res}}\in\mathcal{L}_\infty$, i.e.,

$\sup_{t\geq 0}\|\Theta\boldsymbol{\tau}_{\text{res}}\|_2 < \infty$. Then the smallest path integral $R(t) = \int_{P_1}^{P_2} \|\Theta\delta\boldsymbol{s}\|_2$ exponentially converges to the following error ball:[51]

$$\lim_{t\to\infty} R(t) \leq \sup_{\boldsymbol{s},t} \frac{\|\Theta\boldsymbol{\tau}_{\text{res}}\|_2}{\lambda_{\text{conv,robust}}}\,. \tag{15}$$

Let $\boldsymbol{\tau}_{\text{res}} \in \mathcal{L}_{pe}$, where $\mathcal{L}_{pe}$ is defined as the $\mathcal{L}_p$ norm in the extended space of $p \in [1,\infty]$ as follows:[51]

$$\|(\boldsymbol{\tau}_{\text{res}})_\tau\|_{\mathcal{L}_p} = \left(\int_0^\tau \|\boldsymbol{\tau}_{\text{res}}(t)\|_2^p\, dt\right)^{1/p} < \infty, \quad p \in [1,\infty)\,, \tag{16}$$

$$\|(\boldsymbol{\tau}_{\text{res}})_\tau\|_{\mathcal{L}_\infty} = \sup_{t\geq 0} \|(\boldsymbol{\tau}_{\text{res}}(t))_\tau\|_2 < \infty\,, \tag{17}$$

where $(\boldsymbol{\tau}_{\text{res}})_\tau$ is a truncation of $\boldsymbol{\tau}_{\text{res}}(t)$, i.e., $(\boldsymbol{\tau}_{\text{res}}(t))_\tau = 0$ for $t \geq \tau$, $\tau \in [0,\infty)$ while $(\boldsymbol{\tau}_{\text{res}}(t))_\tau = \boldsymbol{\tau}_{\text{res}}(t)$ for $0 \leq t \leq \tau$. Then the closed-loop system if finite-gain $\mathcal{L}_p$ stable with $p \in [1,\infty]$ for an output function $\boldsymbol{y} = \boldsymbol{h}(\boldsymbol{s}, \boldsymbol{\tau}_{\text{res}}, t)$ with $\int_{Y_1}^{Y_2} \|\delta\boldsymbol{y}\|_2 \leq \eta_1 \int_{P_1}^{P_2} \|\delta\boldsymbol{s}\|_2 + \eta_2\|\boldsymbol{\tau}_{\text{res}}\|_2$, $\exists\eta_1,\eta_2 \geq 0$, since[51]

$$\left\|\left(\int_{Y_1}^{Y_2} \|\delta\boldsymbol{y}\|_2\right)_\tau\right\|_{\mathcal{L}_p} \leq \frac{\eta_1\zeta R(0)}{\sqrt{\lambda_{\min}(\hat{\boldsymbol{M}}(\hat{\boldsymbol{q}}))}} + \left(\frac{\eta_1}{\lambda_{\text{conv,robust}}} + \eta_2\right)\frac{\|(\Theta\boldsymbol{\tau}_{\text{res}})_\tau\|_2}{\sqrt{\lambda_{\min}(\hat{\boldsymbol{M}}(\hat{\boldsymbol{q}}))}}\,, \quad \forall\tau \in [0,\infty)\,, \tag{18}$$

where $Y_1(t)$ and $Y_2(t)$ denote the output trajectories of the original contracting system and its perturbed system respectively and $\zeta = 1$ if $p = \infty$ or $\zeta = 1/(\lambda_{\text{conv,robust}}p)^{1/p}$ if $p \in [1,\infty)$. Note that the perturbed system is also input-to-state stable (ISS).[51]

1. *Design of the Desired MRP Trajectory*

The desired (reference) MRP trajectory $\boldsymbol{q}_d(t)$ is designed such that the asteroid and spacecraft combination stabilizes and reaches the desired attitude orientation $\boldsymbol{q}_{\text{final}}$ in a fuel-optimal fashion. Therefore the desired MRP trajectory can be found by solving the following nonlinear optimal control problem:

$$\begin{aligned}
&\min_{\boldsymbol{q}_d(t),\,\boldsymbol{\omega}_d(t),\,\boldsymbol{u}_d(t)} \int_0^{t_{\text{final}}} \|\boldsymbol{u}_d(t)\|_1 dt\,, \\
\text{subject to}\quad &\hat{\boldsymbol{J}}_{\text{tot}}^{B_{CM}}\dot{\boldsymbol{\omega}}_d(t) - \left(\hat{\boldsymbol{J}}_{\text{tot}}^{B_{CM}}\boldsymbol{\omega}_d(t)\right)\times\boldsymbol{\omega}_d(t) - \hat{\boldsymbol{B}}\boldsymbol{u}_d(t) = 0\,, \\
&\dot{\boldsymbol{q}}_d(t) = \boldsymbol{Z}(\boldsymbol{q}_d(t))\boldsymbol{\omega}_d(t)\,, \\
&\|\boldsymbol{u}_d(t)\|_\infty \leq u_{\max}\,, \qquad \|\boldsymbol{\omega}_d(t)\|_2 \leq \varepsilon_{\text{trans}}\,, \\
&\boldsymbol{\omega}_d(0) = \boldsymbol{\omega}_{\text{init}}\,, \qquad \boldsymbol{\omega}_d(t_{\text{final}}) = \boldsymbol{0}\,, \\
&\boldsymbol{q}_d(0) = \boldsymbol{q}_{\text{init}}\,, \qquad \boldsymbol{q}_d(t_{\text{final}}) = \boldsymbol{q}_{\text{final}}\,.
\end{aligned} \tag{19}$$

In Refs. 40, 54, 55, 56, 57, a number of optimization strategies are discussed for finding these fuel-optimal trajectories.

It is shown in Fig. 6(e) (Section V) that a comparatively negligible amount of fuel is needed for orientating the system to the desired attitude after the angular velocity of the system has stabilized. In this paper, we first find only the fuel-optimal angular velocity trajectory that stabilizes the system and control the system using this desired trajectory. Once the angular velocity of the system is sufficiently close to zero, we augment this fuel-optimal angular velocity trajectory to achieve convergence to the desired attitude. The desired fuel-optimal angular velocity trajectory $\boldsymbol{\omega}_d(t)$ is obtained by solving the following reduced nonlinear optimal control problem:

$$\min_{\boldsymbol{\omega}_d(t),\,\boldsymbol{u}_d(t)} \int_0^{t_{\text{final}}} \|\boldsymbol{u}_d(t)\|_1 dt\,, \tag{20}$$
$$\text{subject to} \quad \hat{\boldsymbol{J}}_{\text{tot}}^{B_{CM}} \dot{\boldsymbol{\omega}}_d(t) - \left(\hat{\boldsymbol{J}}_{\text{tot}}^{B_{CM}} \boldsymbol{\omega}_d(t)\right) \times \boldsymbol{\omega}_d(t) - \hat{\boldsymbol{B}} \boldsymbol{u}_d(t) = 0\,,$$
$$\|\boldsymbol{u}_d(t)\|_\infty \leq u_{\max}\,, \qquad \|\boldsymbol{\omega}_d(t)\|_2 \leq \varepsilon_{\text{trans}}\,,$$
$$\boldsymbol{\omega}_d(0) = \boldsymbol{\omega}_{\text{init}}\,, \qquad \boldsymbol{\omega}_d(t_{\text{final}}) = \boldsymbol{0}\,.$$

Since the reduced nonlinear optimal control problem to find $\boldsymbol{\omega}_d(t)$ in Eq. (20) has fewer constraints compared to the full nonlinear optimal control problem to find both $\boldsymbol{q}_d(t)$ and $\boldsymbol{\omega}_d(t)$ in Eq. (19), it is guaranteed that the solution of the reduced nonlinear optimal control problem in Eq. (20) consumes less fuel than the full nonlinear optimal control problem in Eq. (19).

The desired MRP trajectory $\boldsymbol{q}_d(t)$ is then obtained using the following equations:

$$\dot{\boldsymbol{q}}_d(t) = Z(\boldsymbol{q}_d(t))\boldsymbol{\omega}_d(t)\,, \tag{21}$$
$$\ddot{\boldsymbol{q}}_d(t) = \dot{Z}(\boldsymbol{q}_d(t))\boldsymbol{\omega}_d(t) + Z(\boldsymbol{q}_d(t))\dot{\boldsymbol{\omega}}_d(t)\,, \tag{22}$$

Note that the desired MRP trajectory $\boldsymbol{q}_d(t)$ obtained using Eqs. (21,22) only stabilizes the angular velocity of the system.

Once the angular velocity of the system is sufficiently close to zero, the desired angular velocity trajectory $\boldsymbol{\omega}_d(t)$ is augmented with a damping term so that the system's attitude converges to the desired attitude:

$$\tilde{\boldsymbol{\omega}}_d(t) = \boldsymbol{\omega}_d(t) - k_{qd} Z(\boldsymbol{q}_d(t))^{-1}(\boldsymbol{q}_d(t) - \boldsymbol{q}_{\text{final}})\,, \tag{23}$$

where $k_{qd} > 0$. The desired MRP trajectory $\boldsymbol{q}_d(t)$ is then obtained from the augmented angular velocity $\tilde{\boldsymbol{\omega}}_d(t)$ using the following equations:

$$\dot{\boldsymbol{q}}_d(t) = Z(\boldsymbol{q}_d(t))\tilde{\boldsymbol{\omega}}_d(t) = Z(\boldsymbol{q}_d(t))\boldsymbol{\omega}_d(t) - k_{qd}(\boldsymbol{q}_d(t) - \boldsymbol{q}_{\text{final}})\,, \tag{24}$$
$$\ddot{\boldsymbol{q}}_d(t) = \frac{d}{dt} Z(\boldsymbol{q}_d(t))\tilde{\boldsymbol{\omega}}_d(t) = \dot{Z}(\boldsymbol{q}_d(t))\boldsymbol{\omega}_d(t) + Z(\boldsymbol{q}_d(t))\dot{\boldsymbol{\omega}}_d(t) - k_{qd}\dot{\boldsymbol{q}}_d(t)\,. \tag{25}$$

These equations are initialized and periodically reset using the current MRP $\boldsymbol{q}(t)$ values.

B. Adaptive Nonlinear Tracking Control Law

The robust nonlinear tracking control law Eq. (13) is extended to adaptively estimate the unknown parameters while guaranteeing exponential stability of the modified EL system with uncertainties (12). Let the parameter $\hat{\boldsymbol{a}}$ capture the six uncertain terms in the inertia tensor $\boldsymbol{J}_{\text{tot}}^{B_{CM}}$ using the following equation:[35]

$$\boldsymbol{Y}\hat{\boldsymbol{a}} = \hat{\boldsymbol{M}}(\hat{\boldsymbol{q}})\ddot{\boldsymbol{q}}_r + \hat{\boldsymbol{C}}(\hat{\boldsymbol{q}}, \dot{\hat{\boldsymbol{q}}})\dot{\boldsymbol{q}}_r\,, \tag{26}$$

where $\hat{\boldsymbol{M}}(\hat{\boldsymbol{q}})$, $\hat{\boldsymbol{C}}(\hat{\boldsymbol{q}}, \dot{\hat{\boldsymbol{q}}})$, $\ddot{\boldsymbol{q}}_r$, and $\dot{\boldsymbol{q}}_r$ are defined in Eq. (13). The resulting adaptive nonlinear tracking control law and the tuning law are given by:[35]

$$\hat{\boldsymbol{\tau}}_c = \boldsymbol{Y}\hat{\boldsymbol{a}} - \boldsymbol{K}_r\boldsymbol{s}\,, \tag{27}$$
$$\dot{\hat{\boldsymbol{a}}} = -\boldsymbol{\Gamma}_r \text{Proj}(\hat{\boldsymbol{a}}, \boldsymbol{Y}^T\boldsymbol{s})\,, \tag{28}$$

where the positive-definite matrix $\boldsymbol{K}_r \in \mathbb{R}^{3\times3}$ is the feedback gain and $\boldsymbol{\Gamma}_r \in \mathbb{R}^{6\times6}$ is a positive-definite diagonal matrix. For some boundary function $f(\boldsymbol{\theta})$ (e.g., $f(\boldsymbol{\theta}) = \frac{(\boldsymbol{\theta}^T\boldsymbol{\theta} - \theta_{\max}^2)}{\epsilon_\theta \theta_{\max}^2}$), the projection operator is given by:

$$\text{Proj}(\boldsymbol{\theta}, \boldsymbol{x}) = \begin{cases} \boldsymbol{x} - \frac{\nabla f(\boldsymbol{x}) \nabla f(\boldsymbol{\theta})^T}{\|\nabla f(\boldsymbol{\theta})\|^2} \boldsymbol{x} f(\boldsymbol{\theta}) & \text{if } f(\boldsymbol{\theta}) > 0 \text{ and } \nabla f(\boldsymbol{\theta})^T \boldsymbol{x} > 0 \\ \boldsymbol{x} & \text{otherwise} \end{cases}. \tag{29}$$

A damping term can be added to Eq. (28) to ensure exponential convergence outside this boundary. The proof of global exponential stability of the modified EL system with uncertainties (12) using the adaptive nonlinear tracking control law Eqs. (27,28) is given in Ref. 51.

C. Derivative plus Proportional-Derivative Control Strategy

We now investigate the benefits of simple linear control laws that do not use the dynamics of the system in the control law equation. We first use the derivative (rate damping) linear control law that guarantees global exponential stability for despinning the tumbling asteroid and spacecraft combination. As shown later in Fig. 6(f) (Section V), the majority of the control effort is used for despinning the tumbling system. Once the angular velocity (spin rate) of the asteroid and spacecraft combination is sufficiently close to zero, a proportional-derivative linear control law is used to stabilize the attitude of the asteroid and spacecraft combination in the desired orientation. Note that the proportional-derivative linear control law only guarantees global asymptotic stability of the system. Fortunately, the realistic external disturbances and modeling errors are benign and the system converges to the desired attitude as shown in Section V.

1. *Global Exponential Stability of Derivative Control Law*

We first despin the asteroid and spacecraft combination using the derivative (rate damping) control law given below:

$$\hat{\boldsymbol{B}}\hat{\boldsymbol{u}} = -\boldsymbol{K}_d\hat{\boldsymbol{\omega}}\,, \tag{30}$$

where the positive-definite symmetric matrix $\boldsymbol{K}_d \in \mathbb{R}^{3\times3}$ is the damping gain. We now present the global exponential stability proof of the dynamics of the asteroid and spacecraft combination with uncertainties (11) using this control law. The closed loop dynamics (without $\tilde{\boldsymbol{d}}_{\text{res}}$) can be written as:

$$(\hat{\boldsymbol{J}}_{\text{tot}}^{B_{CM}} + \Delta\boldsymbol{J}_{\text{tot}}^{B_{CM}})\dot{\hat{\boldsymbol{\omega}}} = (\hat{\boldsymbol{J}}_{\text{tot}}^{B_{CM}} + \Delta\boldsymbol{J}_{\text{tot}}^{B_{CM}})\hat{\boldsymbol{\omega}}\times\hat{\boldsymbol{\omega}} - \boldsymbol{K}_d\hat{\boldsymbol{\omega}}\,. \tag{31}$$

Note that $\boldsymbol{J}_{\text{tot}}^{B_{CM}} = (\hat{\boldsymbol{J}}_{\text{tot}}^{B_{CM}} + \Delta\boldsymbol{J}_{\text{tot}}^{B_{CM}})$. Let us review the well-known result of global exponential stability using the Lyapunov function:[41,42,50]

$$V_d = \hat{\boldsymbol{\omega}}^T\boldsymbol{J}_{\text{tot}}^{B_{CM}}\hat{\boldsymbol{\omega}}\,. \tag{32}$$

Differentiating V_d with respect to time gives:

$$\dot{V}_d = (\boldsymbol{J}_{\text{tot}}^{B_{CM}}\hat{\boldsymbol{\omega}}\times\hat{\boldsymbol{\omega}})^T\hat{\boldsymbol{\omega}} - \hat{\boldsymbol{\omega}}^T\boldsymbol{K}_d^T\hat{\boldsymbol{\omega}} + \hat{\boldsymbol{\omega}}^T(\boldsymbol{J}_{\text{tot}}^{B_{CM}}\hat{\boldsymbol{\omega}}\times\hat{\boldsymbol{\omega}}) - \hat{\boldsymbol{\omega}}^T\boldsymbol{K}_d\hat{\boldsymbol{\omega}} = -\hat{\boldsymbol{\omega}}^T(\boldsymbol{K}_d^T + \boldsymbol{K}_d)\hat{\boldsymbol{\omega}}\,, \tag{33}$$

where we used $\hat{\boldsymbol{\omega}}^T(\boldsymbol{J}_{\text{tot}}^{B_{CM}}\hat{\boldsymbol{\omega}}\times\hat{\boldsymbol{\omega}}) = 0$. Let $\lambda_{\min}(\boldsymbol{K}_d) = k_{1d}$. Therefore:

$$\dot{V}_d \le -2k_{1d}\|\hat{\boldsymbol{\omega}}\|_2^2 \le -\frac{2k_{1d}}{\lambda_{\max}(\boldsymbol{J}_{\text{tot}}^{B_{CM}})}V_d\,. \tag{34}$$

It follows from the comparison lemma that the solution of $\hat{\boldsymbol{\omega}}(t)$ is defined for all time and satisfies:[53]

$$\|\hat{\boldsymbol{\omega}}(t)\|_2 \le e^{-k_{1d}t}\|\hat{\boldsymbol{\omega}}(0)\|_2\,. \tag{35}$$

Thus, the angular velocity of the system converge exponentially fast to $\boldsymbol{0}$, regardless of initial conditions, with the convergence rate of $\lambda_{\min}(\boldsymbol{K}_d)$. Moreover, in the presence of disturbance $\tilde{\boldsymbol{d}}_{\text{res}}$ bounded by $\|\tilde{\boldsymbol{d}}_{\text{res}}\|_2 \le \tilde{d}_{\text{res,max}}$, the nonvanishing perturbation lemma states that the solution of the perturbed system $\hat{\boldsymbol{\omega}}(t)$ exponentially converges to the following error ball:[53]

$$\|\hat{\boldsymbol{\omega}}(t)\|_2 \le \frac{\lambda_{\max}(\boldsymbol{J}_{\text{tot}}^{B_{CM}})}{k_{1d}\lambda_{\min}(\boldsymbol{J}_{\text{tot}}^{B_{CM}})}\tilde{d}_{\text{res,max}}\,. \tag{36}$$

This control law is used to reduce the angular velocity of the system till it is approximately equal to the angular velocity measurement error ($\Delta\boldsymbol{\omega}$).

2. Global Asymptotic Stability of Proportional-Derivative Control Law

Once the angular velocity (spin rate) of the asteroid and spacecraft combination is sufficiently close to zero, i.e. below the threshold of the angular velocity measurement error ($\Delta\boldsymbol{\omega}$), then the following proportional-derivative control law is used to control both the attitude kinematics and dynamics of the asteroid and spacecraft combination:

$$\hat{\boldsymbol{B}}\hat{\boldsymbol{u}} = -k_p\boldsymbol{\beta}_{\text{error},v} - \boldsymbol{K}_d\hat{\boldsymbol{\omega}}\,, \tag{37}$$

where the constant $k_p > 0$ is the feedback gain and the error quaternion $(\boldsymbol{\beta}_{\text{error},v}, \boldsymbol{\beta}_{\text{error},4}) \in \mathbb{R}^3 \times \mathbb{R}$ represents the orientation error of $\mathcal{F}_B$ with respect to the desired target attitude $\boldsymbol{\beta}_{\text{final}}$. It is shown in Section V that a comparatively negligible amount of fuel is needed for stabilizing the attitude.

We now show the global asymptotic stability of this control law for the attitude kinematics (4) and dynamics (11) of the asteroid and spacecraft combination. The closed loop system (without $\tilde{\boldsymbol{d}}_{\text{res}}$) can be written as:[31]

$$\dot{\boldsymbol{\beta}}_{\text{error},v} = \frac{1}{2}(\boldsymbol{\beta}_{\text{error},4}\hat{\boldsymbol{\omega}} + \boldsymbol{\beta}_{\text{error},v} \times \hat{\boldsymbol{\omega}})\,, \tag{38}$$

$$\dot{\boldsymbol{\beta}}_{\text{error},4} = -\frac{1}{2}\boldsymbol{\beta}^T_{\text{error},v}\hat{\boldsymbol{\omega}}\,, \tag{39}$$

$$(\hat{\boldsymbol{J}}^{B_{CM}}_{\text{tot}} + \Delta\boldsymbol{J}^{B_{CM}}_{\text{tot}})\dot{\hat{\boldsymbol{\omega}}} = (\hat{\boldsymbol{J}}^{B_{CM}}_{\text{tot}} + \Delta\boldsymbol{J}^{B_{CM}}_{\text{tot}})\hat{\boldsymbol{\omega}} \times \hat{\boldsymbol{\omega}} - k_p\boldsymbol{\beta}_{\text{error},v} - \boldsymbol{K}_d\hat{\boldsymbol{\omega}}\,. \tag{40}$$

Let the Lyapunov function be given by:[41,42,50]

$$\begin{aligned} V_{pd} &= \hat{\boldsymbol{\omega}}^T\boldsymbol{J}^{B_{CM}}_{\text{tot}}\hat{\boldsymbol{\omega}} + 2k_p\boldsymbol{\beta}^T_{\text{error},v}\boldsymbol{\beta}_{\text{error},v} + 2k_p(1-\boldsymbol{\beta}_{\text{error},4})^2\,, \\ &= \hat{\boldsymbol{\omega}}^T\boldsymbol{J}^{B_{CM}}_{\text{tot}}\hat{\boldsymbol{\omega}} + 4k_p(1-\boldsymbol{\beta}_{\text{error},4})\,, \end{aligned} \tag{41}$$

where we simplified V_{pd} using the condition $\boldsymbol{\beta}^T_{\text{error},v}\boldsymbol{\beta}_{\text{error},v} + \boldsymbol{\beta}^2_{\text{error},4} = 1$. Differentiating V_{pd} with respect to time gives:

$$\dot{V}_{pd} = -\hat{\boldsymbol{\omega}}^T\boldsymbol{K}^T_d\hat{\boldsymbol{\omega}} - \hat{\boldsymbol{\omega}}^T\boldsymbol{K}_d\hat{\boldsymbol{\omega}} - k_p\boldsymbol{\beta}^T_{\text{error},v}\hat{\boldsymbol{\omega}} - k_p\hat{\boldsymbol{\omega}}^T\boldsymbol{\beta}_{\text{error},v} + 2k_p\boldsymbol{\beta}^T_{\text{error},v}\hat{\boldsymbol{\omega}} = -\hat{\boldsymbol{\omega}}^T(\boldsymbol{K}^T_d + \boldsymbol{K}_d)\hat{\boldsymbol{\omega}}\,. \tag{42}$$

Since the right hand side is a positive semi-definite matrix, the angular velocity and the attitude error asymptotically converge to $\boldsymbol{0}$ and $(\boldsymbol{0}, +1)$ respectively using this proportional-derivative control law. Note that the global asymptotic stability of the proportional-derivative control law for the modified EL system (12) is shown in Refs. 52, 58.

Thus, we have presented three control laws that guarantee global exponential or asymptotic stability of the asteroid and spacecraft combination. In the next section we numerically compare the performance of these three control laws.

V. Simulation Results

In this section, we first numerically compare the performance of the three control laws discussed in Section IV: the robust nonlinear tracking control law Eq. (13), the adaptive nonlinear tracking control law Eqs. (27,28), and the derivative plus proportional-derivative control strategy Eqs. (30,37). We then present a detailed sensitivity analysis of the derivative plus proportional-derivative control strategy.

A. Comparison of Control Laws for Attitude Control and Stabilization

The block diagram representation of the simulation setup is shown in Fig 5. The plant model represents the attitude kinematics (4) and dynamics (2) of the asteroid and spacecraft combination. The measured attitude $\hat{\boldsymbol{q}}$ and angular velocity $\hat{\boldsymbol{\omega}}$ are used by the control law to generate the control inputs $\hat{\boldsymbol{\tau}}_c$ or $\hat{\boldsymbol{B}}\hat{\boldsymbol{u}}$.

The best strategy for allocating thrusts to the eight RCS thrusters, from the calculated control input $\hat{\boldsymbol{\tau}}_c$, is to solve the following optimization problem:

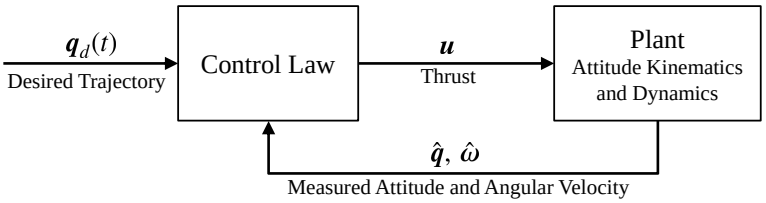

Figure 5: Block diagram representation of the simulation setup.

$$\begin{aligned} &\min_{\hat{\boldsymbol{u}}} \|\hat{\boldsymbol{u}}\|_1 \\ \text{subject to} \quad &\hat{\boldsymbol{\tau}}_c = \boldsymbol{Z}^{-T}(\hat{\boldsymbol{q}})\hat{\boldsymbol{B}}\hat{\boldsymbol{u}}\,, \\ &\|\hat{\boldsymbol{u}}\|_\infty \leq u_{\max}\,. \end{aligned} \tag{43}$$

The optimal thrust allocation problem in Eq. (43) can be solved at every time instant using linear programming. Instead, in this paper, we use the Moore–Penrose pseudoinverse to allocate thrusts to the eight RCS thrusters as shown below:

$$\hat{\boldsymbol{u}} = \hat{\boldsymbol{B}}^T \left(\hat{\boldsymbol{B}}\hat{\boldsymbol{B}}^T\right)^{-1} \boldsymbol{Z}^T(\hat{\boldsymbol{q}})\hat{\boldsymbol{\tau}}_c\,. \tag{44}$$

Note that we use the right-pseudoinverse since the matrix $\hat{\boldsymbol{B}}$ has full row rank and the matrix inverse $\left(\hat{\boldsymbol{B}}\hat{\boldsymbol{B}}^T\right)^{-1}$ is well defined. We do not recommend using the left-pseudoinverse since the matrix $\left(\hat{\boldsymbol{B}}^T\hat{\boldsymbol{B}}\right)$ is usually near singular and hence its inverse may not be defined.

The resulting control input $\boldsymbol{u}$ is then sent to the plant. The fuel consumed by the conceptual ARM spacecraft, from time t_0 to t_f, is computed using the following equation:

$$\text{Fuel consumed} = \frac{1}{I_{sp}\, g_0} \int_{t_0}^{t_f} \|\boldsymbol{u}\|_1 dt\,, \tag{45}$$

where I_{sp} is the specific impulse of the fuel in the RCS thrusters (i.e., 287 sec for the conceptual ARM spacecraft[6]) and g_0 is the nominal acceleration due to the gravity (i.e., 9.8 m sec^{-2}).

In this section, we assume that the ARM spacecraft, whose nominal design is presented in Section II.A, captures the 1.2×10^6 kg asteroid and stabilizes the rigid asteroid and spacecraft combination from the given initial conditions to the desired final conditions. The simulation parameters used in this section are given in Table 5. We assume that the actuators of the ARM spacecraft are precisely calibrated, hence there is no actuator noise.

Table 6 shows the performance of three control laws under varying levels of: (i) modeling uncertainties in the estimated inertia tensor of the asteroid ($\Delta \boldsymbol{J}_{\text{ast}}^{B_{CM}}$), (ii) modeling uncertainties in the vector from the base of the ARM-spacecraft's body to the center of mass of the system ($\Delta \boldsymbol{r}^{S_O/B_{CM}}$), (iii) measurement errors in the system's angular velocity ($\Delta\boldsymbol{\omega}$), (iv) measurement errors in the system's attitude represented using MRP ($\Delta\boldsymbol{q}$), and (v) actuator saturations ($u_{\max}$). Each simulation is executed for 10^5 sec ($\approx$ 28 hours). Some of the terms used in Table 6 are described below:

- The additive measurement errors ($\Delta\boldsymbol{\omega}$, $\Delta\boldsymbol{q}$) are simulated using band-limited white noise where $\mathcal{P}(\cdot)$ specifies the height of the power spectral density of the white noise, which is the same for each axis.
- The angular velocity convergence time $t_{\omega,\text{conv}}$ denotes the least time instant after which the system's angular velocity $\boldsymbol{\omega}(t)$ is always below the given threshold of 10^{-4} rad sec^{-1}, i.e., $\|\boldsymbol{\omega}(t)\|_2 \leq 10^{-4}$ rad sec^{-1}, $\forall t > t_{\omega,\text{conv}}$.
- The attitude convergence time $t_{q,\text{conv}}$ denotes the least time instant after which the error in the EL system's attitude $\|\boldsymbol{q}(t) - \boldsymbol{q}_{\text{final}}\|_2$ is always below the given threshold of 10^{-2}, i.e., $\|\boldsymbol{q}(t) - \boldsymbol{q}_{\text{final}}\|_2 \leq 10^{-2}$, $\forall t > t_{q,\text{conv}}$. Note that after time $t_{q,\text{conv}}$, the control law can be switched off as the asteroid and spacecraft combination has been three-axis stabilized in the final desired orientation. The fuel consumed up to time $t_{\omega,\text{conv}}$ and $t_{q,\text{conv}}$ are also shown in Table 6.

Table 5: Simulation parameters

Type of Parameter	Value
Conceptual ARM Spacecraft Parameters	$m_{\text{sc}} = 1.6 \times 10^4$ kg, $\boldsymbol{J}_{\text{sc}}^{S_{CM}} = 10^4 \times \begin{bmatrix} 5.584 & 0 & 0 \\ 0 & 5.584 & 0 \\ 0 & 0 & 1.568 \end{bmatrix}$ kg m^2, $\boldsymbol{r}^{S_{CM}/S_O} = [\ 0 \quad 0 \quad 3.0\ ]$ m,
Asteroid Parameters	$m_{\text{ast}} = 1.2 \times 10^6$ kg, $\rho_{\text{ast}} = 1.9$ g cm^{-3}, Shape model: Eros, $\boldsymbol{J}_{\text{ast}}^{B_{CM}} = 10^7 \times \begin{bmatrix} 0.8658 & 0.4432 & -0.0005 \\ 0.4432 & 3.4900 & 0.0002 \\ -0.0005 & 0.0002 & 3.5579 \end{bmatrix}$ kg m^2, $\boldsymbol{r}^{S_O/B_{CM}} = [\ -0.0495 \quad -0.0004 \quad 3.5456\ ]$ m,
External Disturbance Actuator Error	$\|\boldsymbol{d}_{\text{ext}}\|_2 \approx 1$ Nm, $\Delta\boldsymbol{u} = 0$ N,
Initial Conditions	$\boldsymbol{q}_{\text{initial}} = [\ 0.05 \quad 0.04 \quad 0.03\ ]$, $\boldsymbol{\omega}_{\text{initial}} = [\ 0.01 \quad 0.02 \quad 0.03\ ]$ rad sec^{-1},
Desired Final Conditions Eqs. (7,8)	$\|\boldsymbol{\omega}(t)\|_2 \leq 0.5$ rpm, $\forall t \in \mathbb{R}$, $\boldsymbol{q}_{\text{final}} = [\ 0 \quad 0 \quad 0\ ]$, $\|\boldsymbol{q}(t) - \boldsymbol{q}_{\text{final}}\|_2 \leq 10^{-2}$, $\forall t > 10^5$ sec, $\|\boldsymbol{\omega}(t)\|_2 \leq 10^{-4}$ rad sec^{-1}, $\forall t > 10^5$ sec,
Robust Nonlinear Tracking Control Law Eq. (13)	$\boldsymbol{K}_r = 10^3 \times \mathbf{I}$, $\boldsymbol{\Lambda}_r = 10 \times \mathbf{I}$, Desired angular velocity $\boldsymbol{\omega}_d(t)$ is obtained by solving Eq. (20) using the GPOPS-II numerical solver[59,60] Desired MRP trajectory $\boldsymbol{q}_d(t)$ obtained using Eqs. (21,22), When $\|\boldsymbol{\omega}(t)\|_2 \leq 5 \times 10^{-4}$ rad sec^{-1}, switch to augmented angular velocity $\tilde{\boldsymbol{\omega}}_d(t)$ in Eq. (23) with $k_{qd} = 10^{-4}$, Desired MRP trajectory $\boldsymbol{q}_d(t)$ obtained using Eqs. (24,25),
Adaptive Nonlinear Tracking Control Law Eqs. (27,28)	Same as above and $\boldsymbol{\Gamma}_r = 10^{12} \times \mathbf{I}$,
Derivative plus Proportional-Derivative Control Strategy Eqs. (30,37)	$\boldsymbol{K}_d = 10^4 \times \mathbf{I}$, $k_p = 10$, Switch from derivative to proportional-derivative when $\|\boldsymbol{\omega}(t)\|_2 \leq 5 \times 10^{-4}$ rad sec^{-1}.

- The symbol $\mathcal{NC}$ or "Not Converged" refers to the case when the control law is not able to stabilize the system, which is usually due to actuator saturation.

It is shown in Table 6 that under increasing levels of modeling uncertainties and measurement errors, only the derivative plus proportional-derivative (hereafter referred to as D+PD) control strategy Eqs. (30,37) is able to stabilize the asteroid and spacecraft combination.

It is shown in Case 1 that in the absence of measurement errors and modeling uncertainties, which can be achieved using online system identification, the robust nonlinear tracking control law Eq. (13) tracks the fuel-optimum reference trajectory and consequently consumes less fuel than the D+PD control strategy. The simulation results are shown in Fig. 6(a,c,e). Note that the angular velocity of the asteroid and spacecraft combination converges within 4.44×10^4 sec in Fig. 6(a), i.e., $\|\boldsymbol{\omega}(t)\|_2 \leq 10^{-4}$ rad sec^{-1}, $\forall t > 4.44 \times 10^4$ sec. Similarly, the attitude of the asteroid and spacecraft combination converges within 8.05×10^4 sec in Fig. 6(c), i.e., $\|\boldsymbol{q}(t) - \boldsymbol{q}_{\text{final}}\|_2 \leq 10^{-2}$, $\forall t > 8.05 \times 10^4$ sec. Note that these convergence times can be decreased with higher gain values. Moreover, Fig. 6(e) also shows the fuel consumption for the case where the fuel-optimal $\boldsymbol{\omega}_d(t)$ trajectory is not augmented (i.e., $k_{qd} = 0$) and consequently only the angular velocity of the system converges. We can infer from this plot that a comparatively negligible amount of fuel (≈ 1 kg) is used for stabilizing the attitude of the asteroid and spacecraft combination using the augmented angular

Table 6: Performance of the control laws under varying levels of uncertainties and disturbances.

	System Parameters	**Control Law Performance**			
	Modeling Uncertainty Measurement Errors Actuator Saturation	Convergence Time and Fuel Consumed	Robust$^{\|}$ Nonlinear	Adaptive$^{\#}$ Nonlinear	D+PD†† Linear
1.	$\Delta \boldsymbol{J}_{\text{ast}}^{B_{CM}} = 0$ kg m^2 $\Delta \boldsymbol{r}^{S_O/B_{CM}} = 0$ m $\Delta \boldsymbol{\omega} = 0$ rad sec^{-1} $\Delta \boldsymbol{q} = 0$, $u_{\max} = 200$ N	$t_{\omega,\text{conv}}$**	4.44×10^4 sec	4.54×10^4 sec	3.08×10^4 sec
		Fuel at $t_{\omega,\text{conv}}$	84.9 kg	86.4 kg	120.2 kg
		$t_{q,\text{conv}}$$^{|||}$	8.05×10^4 sec	8.20×10^4 sec	4.31×10^4 sec
		Fuel at $t_{q,\text{conv}}$	100.1 kg	103.2 kg	121.4 kg
2.	$\|\Delta \boldsymbol{J}_{\text{ast}}^{B_{CM}}\|_2 \approx 10^5$ kg m^2 $\|\Delta \boldsymbol{r}^{S_O/B_{CM}}\|_2 \approx 10^{-2}$ m $\Delta \boldsymbol{\omega} = 0$ rad sec^{-1} $\Delta \boldsymbol{q} = 0$, $u_{\max} = 200$ N	$t_{\omega,\text{conv}}$**	5.21×10^4 sec	5.37×10^4 sec	3.16×10^4 sec
		Fuel at $t_{\omega,\text{conv}}$	88.6 kg	90.2 kg	120.6 kg
		$t_{q,\text{conv}}$$^{|||}$	8.51×10^4 sec	8.66×10^4 sec	4.31×10^4 sec
		Fuel at $t_{q,\text{conv}}$	102.4 kg	105.3 kg	121.7 kg
3.	$\|\Delta \boldsymbol{J}_{\text{ast}}^{B_{CM}}\|_2 \approx 10^6$ kg m^2 $\|\Delta \boldsymbol{r}^{S_O/B_{CM}}\|_2 \approx 10^{-1}$ m $\Delta \boldsymbol{\omega} = 0$ rad sec^{-1} $\Delta \boldsymbol{q} = 0$, $u_{\max} = 200$ N	$t_{\omega,\text{conv}}$**	2.28×10^4 sec	2.37×10^4 sec	3.41×10^4 sec
		Fuel at $t_{\omega,\text{conv}}$	97.8 kg	98.4 kg	121.0 kg
		$t_{q,\text{conv}}$$^{|||}$	5.60×10^4 sec	5.69×10^4 sec	4.84×10^4 sec
		Fuel at $t_{q,\text{conv}}$	111.7 kg	112.6 kg	121.6 kg
4.	$\|\Delta \boldsymbol{J}_{\text{ast}}^{B_{CM}}\|_2 \approx 10^7$ kg m^2 $\|\Delta \boldsymbol{r}^{S_O/B_{CM}}\|_2 \approx 1$ m $\Delta \boldsymbol{\omega} = 0$ rad sec^{-1} $\Delta \boldsymbol{q} = 0$, $u_{\max} = 1000$ N	$t_{\omega,\text{conv}}$**	2.80×10^4 sec	2.90×10^4 sec	2.80×10^4 sec
		Fuel at $t_{\omega,\text{conv}}$	555.9 kg	556.1 kg	116.1 kg
		$t_{q,\text{conv}}$$^{|||}$	5.96×10^4 sec	6.07×10^4 sec	4.16×10^4 sec
		Fuel at $t_{q,\text{conv}}$	568.6 kg	570.7 kg	117.5 kg
5.	$\Delta \boldsymbol{J}_{\text{ast}}^{B_{CM}} = 0$ kg m^2 $\Delta \boldsymbol{r}^{S_O/B_{CM}} = 0$ m $\mathcal{P}(\Delta \boldsymbol{\omega}) \approx 10^{-14}$ rad^2 sec^{-2} $\mathcal{P}(\Delta \boldsymbol{q}) \approx 10^{-10}$, $u_{\max} = 1000$ N	$t_{\omega,\text{conv}}$**	4.45×10^4 sec	4.54×10^4 sec	3.08×10^4 sec
		Fuel at $t_{\omega,\text{conv}}$	1026.5 kg	1208.9 kg	120.2 kg
		$t_{q,\text{conv}}$$^{|||}$	8.06×10^4 sec	8.05×10^4 sec	4.31×10^4 sec
		Fuel at $t_{q,\text{conv}}$	1690.7 kg	2031.5 kg	121.4 kg
6.	$\|\Delta \boldsymbol{J}_{\text{ast}}^{B_{CM}}\|_2 \approx 10^7$ kg m^2 $\|\Delta \boldsymbol{r}^{S_O/B_{CM}}\|_2 \approx 1$ m $\mathcal{P}(\Delta \boldsymbol{\omega}) \approx 10^{-8}$ rad^2 sec^{-2} $\mathcal{P}(\Delta \boldsymbol{q}) \approx 10^{-4}$, $u_{\max} = 200$ N	$t_{\omega,\text{conv}}$**	$\mathcal{NC}^{\ddagger\ddagger}$	$\mathcal{NC}^{\ddagger\ddagger}$	2.67×10^4 sec
		Fuel at $t_{\omega,\text{conv}}$			124.4 kg
		$t_{q,\text{conv}}$$^{|||}$	$\mathcal{NC}^{\ddagger\ddagger}$	$\mathcal{NC}^{\ddagger\ddagger}$	4.10×10^4 sec
		Fuel at $t_{q,\text{conv}}$			134.9 kg

$^{\|}$Robust Nonlinear Tracking Control Law Eq. (13)

$^{\#}$Adaptive Nonlinear Tracking Control Law Eqs. (27,28)

††Derivative plus Proportional-Derivative Control Strategy Eqs. (30,37)

‡‡Not Converged

**Angular Velocity Convergence Time $t_{\omega,\text{conv}} \in \mathbb{R}$ such that $\|\boldsymbol{\omega}(t)\|_2 \leq 10^{-4}$ rad sec^{-1}, $\forall t > t_{\omega,\text{conv}}$

$^{\|\|\|}$Attitude Convergence Time $t_{q,\text{conv}} \in \mathbb{R}$ such that $\|\boldsymbol{q}(t) - \boldsymbol{q}_{\text{final}}\|_2 \leq 10^{-2}$, $\forall t > t_{q,\text{conv}}$

velocity trajectory $\tilde{\boldsymbol{\omega}}_d(t)$ in Eq. (23).

We conclude from Cases 2 and 3 that in the absence of measurement errors and under minor modeling uncertainties, which can be achieved using online system identification techniques, the robust nonlinear tracking control law is the best strategy as it guarantees exponential convergence to the fuel-optimal reference trajectory and consumes the least fuel. One caveat of using this control law is that the nonlinear optimal control problem in Eq. (20) should be solved in real time for the given initial angular velocity $\boldsymbol{\omega}_{\text{initial}}$ and the estimated inertia tensor of the asteroid and spacecraft combination $\hat{\boldsymbol{J}}_{\text{tot}}^{B_{CM}}$.

Case 4 in Table 6 shows that the two nonlinear control laws, which use the dynamics of the system in their control law equation, consume more fuel than the D+PD control strategy due to the larger resultant disturbance torque discussed in Section III. Case 5 shows that both the nonlinear control laws consume more fuel than the D+PD control strategy in the presence of measurement errors and the adaptive nonlinear

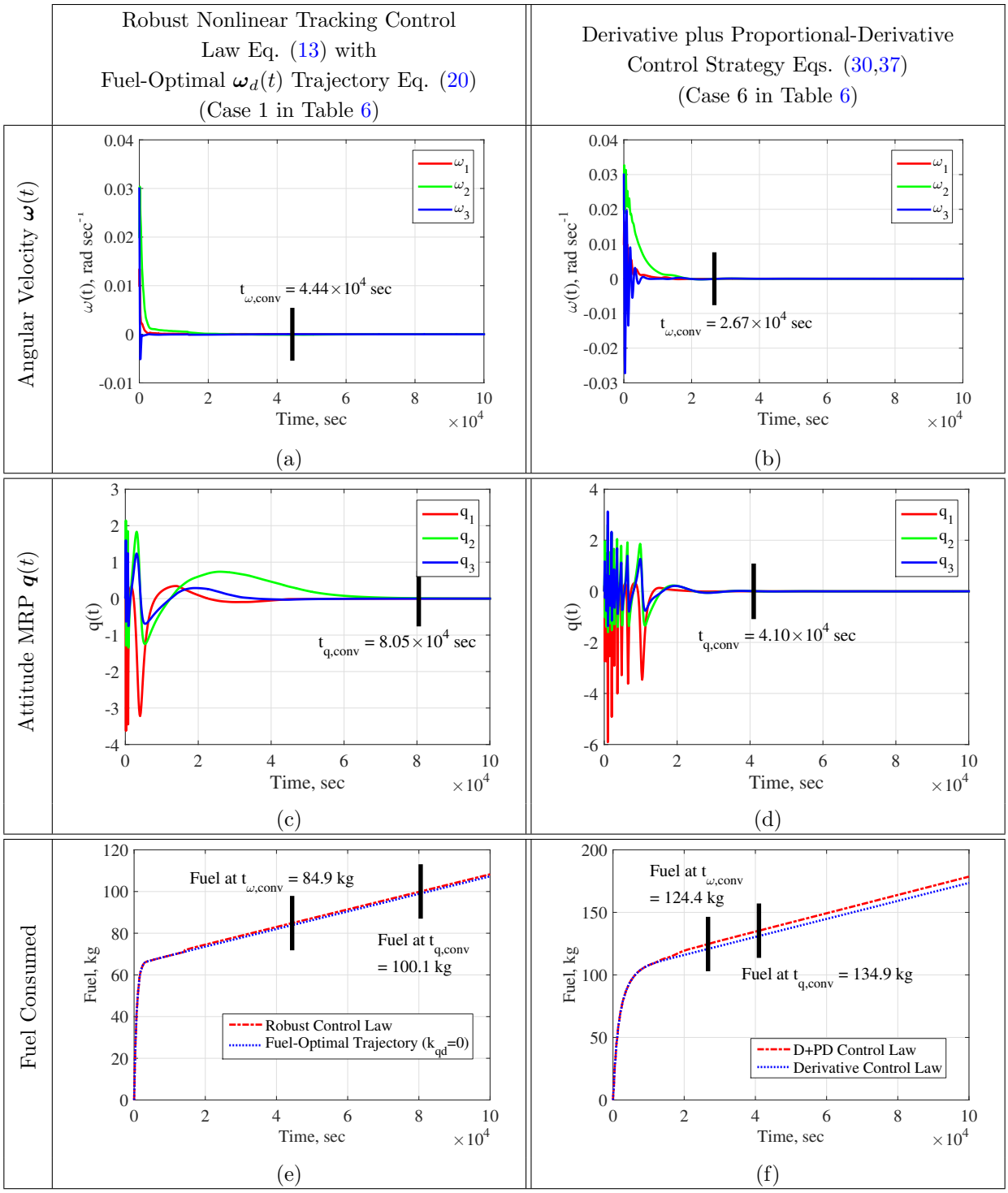

Figure 6: Simulation results of the robust nonlinear tracking control law (Case 1 in Table 6) and the D+PD control strategy (Case 6 in Table 6) are shown. The plots show the trajectories of the angular velocity $\boldsymbol{\omega}(t)$, the attitude represented using MRP $\boldsymbol{q}(t)$, and the fuel consumed with respect to time for the two control laws. The angular velocity convergence time $t_{\omega,\text{conv}}$, the attitude convergence time $t_{q,\text{conv}}$, and the fuel consumed up to these time instants are also shown.

control law is more sensitive to these measurement errors. Moreover these two nonlinear control laws are not capable of handling realistic levels of uncertainties and errors (see Case 6) due to actuator saturation.

Hence we conclude that the robust nonlinear tracking control law Eq. (13) and the adaptive nonlinear tracking control law Eq. (27,28) are not suitable for this control problem in the presence of large modeling uncertainties, measurement errors, and actuator saturations. Note that we have not incorporated filters to accurately estimate the states from the noisy measurements. We envisage that using such filters will significantly improve the performance of these nonlinear control laws in the presence of measurement errors.

In contrast, the D+PD control strategy, which does not use the dynamics of the system in the control law equation, performs well under realistic levels of uncertainties and errors as seen in Case 6. Moreover, the fuel consumed and the time of convergence do not change much with uncertainties and errors, as seen in Cases 1–6. Note that Case 6 shows the worst case measurement errors for the desired convergence bounds. If the measurement errors (noise levels) increase above the values stated in Case 6, then the instantaneous magnitude of the measurement errors become comparable to the desired convergence bounds and the ARM spacecraft expends fuel continuously to counter these errors. Therefore these uncertainty and error limits place requirements on the technical capabilities of the sensors and actuators onboard the actual ARM spacecraft.

The simulation results (trajectories) of the D+PD control strategy, for the simulation parameters in Table 5 and the uncertainty and error limits specified in Case 6 of Table 6, are shown in Fig. 6(b,d,f). Note that the angular velocity of the asteroid and spacecraft combination converges within 2.67×10^4 sec in Fig. 6(b), i.e., $\|\boldsymbol{\omega}(t)\|_2 \leq 10^{-4}$ (rad sec^{-1}), $\forall t > 2.67 \times 10^4$ sec. Similarly, the attitude of the asteroid and spacecraft combination converges within 4.10×10^4 sec in Fig. 6(d), i.e., $\|\boldsymbol{q}(t) - \boldsymbol{q}_{\text{final}}\|_2 \leq 10^{-2}$, $\forall t > 4.10 \times 10^4$ sec. Note that the ARM spacecraft continues to expend fuel, even after the system has stabilized satisfactorily, for countering the measurement errors. But the net fuel consumed is comfortably within the fuel capacity of the conceptual ARM spacecraft (i.e., 900 kg[6]). Figure 6(f) also shows the fuel consumption for the case where only the derivative (rate damping) control law Eq. (30) is used for the entire time and consequently only the angular velocity of the system converges. We can infer from this plot that a comparatively negligible amount of fuel (≈ 5 kg) is used by the proportional term $-k_p \boldsymbol{\beta}_{\text{error},v}$ in Eq. (37) for stabilizing the attitude of the asteroid and spacecraft combination.

B. Sensitivity Analysis of the Derivative plus Proportional-Derivative Control Strategy

We now present detailed sensitivity analysis of the D+PD control strategy by varying the asteroid parameters, the initial conditions, and the control law parameters. In this section, the parameters that are not explicitly specified are taken from Table 5 and Case 6 of Table 6. Figure 7 shows the results of Monte Carlo simulations over a wide range of asteroid parameters. We observe that the D+PD control strategy performs relatively well and the fuel consumed by the conceptual ARM spacecraft is upper bounded by 300 kg for nominal range of asteroid parameters given in Table 1. The maximum fuel is consumed when the asteroid has the largest mass (15×10^5 kg) and smallest density (1.0 g cm^{-3}). But in this case, the asteroid's diameter would be more than 20 m as shown in Fig. 2(c,d), making it an unsuitable target due to the limited size of the ARM-spacecraft's capture mechanism.

Previously, we inferred from Fig. 6(f) that the derivative (rate damping) term $-\boldsymbol{K}_d \hat{\boldsymbol{\omega}}$ in the D+PD control strategy Eqs. (30,37) dictates the fuel consumption and the effect of the proportional term is negligible. The effect of this damping gain, which is given by $\boldsymbol{K_d} = k_d \mathbf{I}$, on the fuel consumption and the convergence time is shown in Fig. 8. Even though k_d is varied from 0.5×10^4-2.5×10^4, its effect on the fuel consumed in 10^5 sec is minimal as shown in Fig. 8(a,b). On the other hand, increasing k_d reduces the convergence time of the angular velocity as shown in Fig. 8(c,d) and the convergence time of the attitude as shown in Fig. 8(e,f). If k_d is chosen less than 0.5×10^4, then the angular-velocity's convergence time increases beyond 10^5 sec, which is not desirable. If k_d is chosen greater than 2.5×10^4, then the system converges quickly but the control action becomes extremely sensitive to the angular velocity measurement error and a lot of fuel is wasted in countering the perceived angular velocity even after the system has stabilized. Hence we recommend that the damping gain $k_d \approx 10^4$ is ideal for this ARM mission concept.

It is seen in Fig. 7(a,b) that the asteroid with mass $m_{\text{ast}} = 1.1 \times 10^6$ kg and density $\rho_{\text{ast}} = 1.9$ g cm^{-3} consumes the maximum fuel among all asteroids in the nominal range. The effect of the initial angular velocity $\boldsymbol{\omega}_{\text{initial}}$ on the fuel consumption and convergence time for this nominal asteroid is shown in Fig. 9. We observe that the fuel consumed by the conceptual ARM spacecraft is upper bounded by 300 kg for all initial conditions, as shown in Fig. 9(a,b). Hence we conclude that the fuel consumed by the conceptual ARM spacecraft using the D+PD control strategy is upper bounded by 300 kg for the nominal range of asteroid parameters, i.e., the asteroid's mass is within 2.5-13 $\times 10^5$ kg, the asteroid's density is within 1.9-3.8 g cm^{-3},

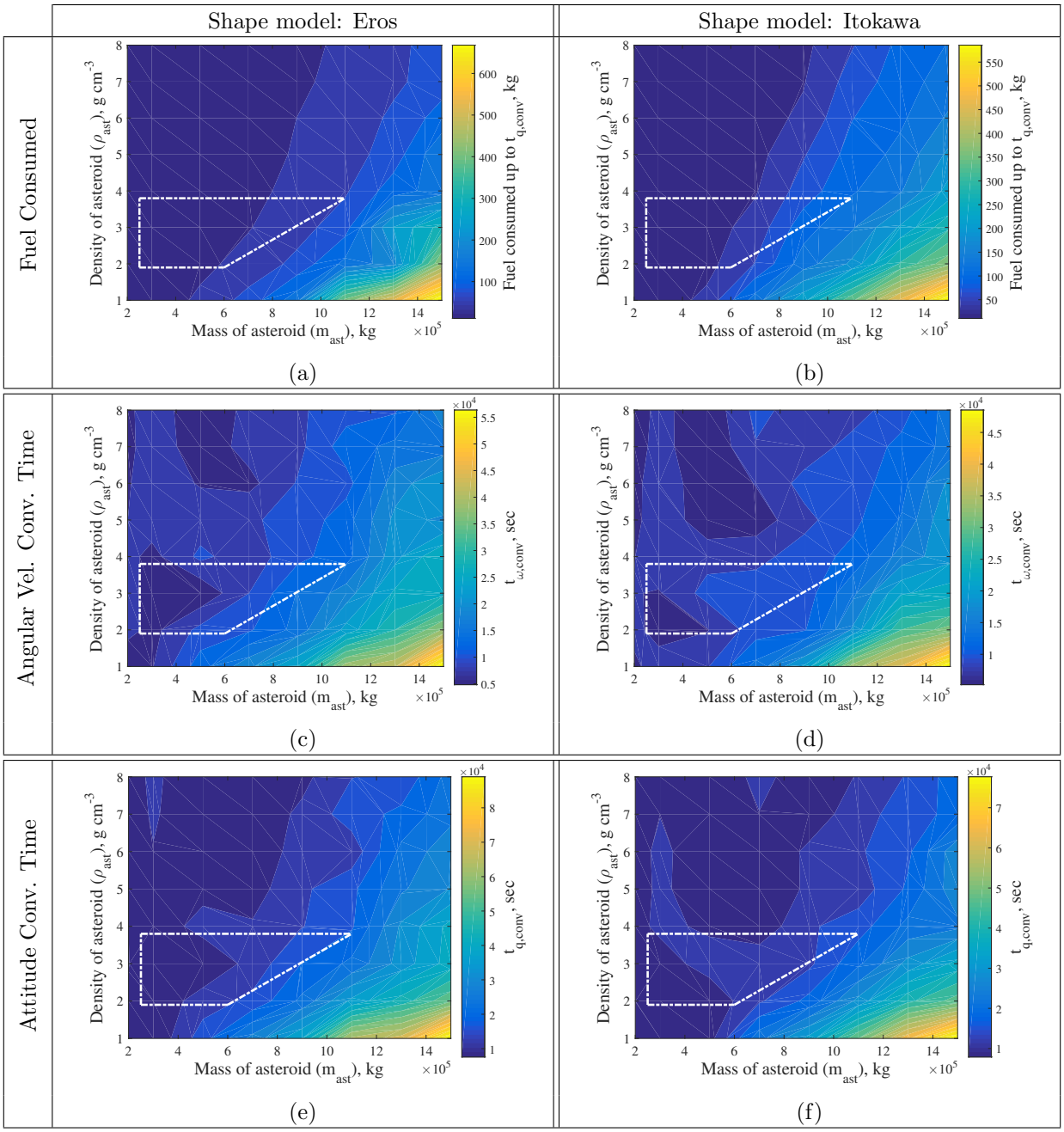

Figure 7: Monte Carlo simulations show the performance of the D+PD control strategy over a wide range of asteroid parameters for the shape models of Eros and Itokawa respectively. The plots show the variation of the convergence time of the angular velocity ($t_{\omega,\text{conv}}$), the convergence time of the attitude ($t_{q,\text{conv}}$), and the fuel consumed up to time $t_{q,\text{conv}}$ with respect to the mass and density of the model asteroid. The inset white trapezium shows the nominal range of NEO asteroid parameters, i.e., the asteroid's mass is within 2.5-13 $\times 10^5$ kg, the asteroid's density is within 1.9-3.8 g cm^{-3}, and the asteroid's diameter is less than 15 m.

and the asteroid's diameter is less than 15 m. Note that the convergence times of the angular velocities and the attitudes are satisfactory for all initial conditions, as shown in Fig. 9(c-f). As discussed previously, the effect of the initial attitude $\boldsymbol{q}_{\text{initial}}$ on the fuel consumption and convergence time is negligible. The design guidelines that can be inferred from these simulation results are discussed in the next section.

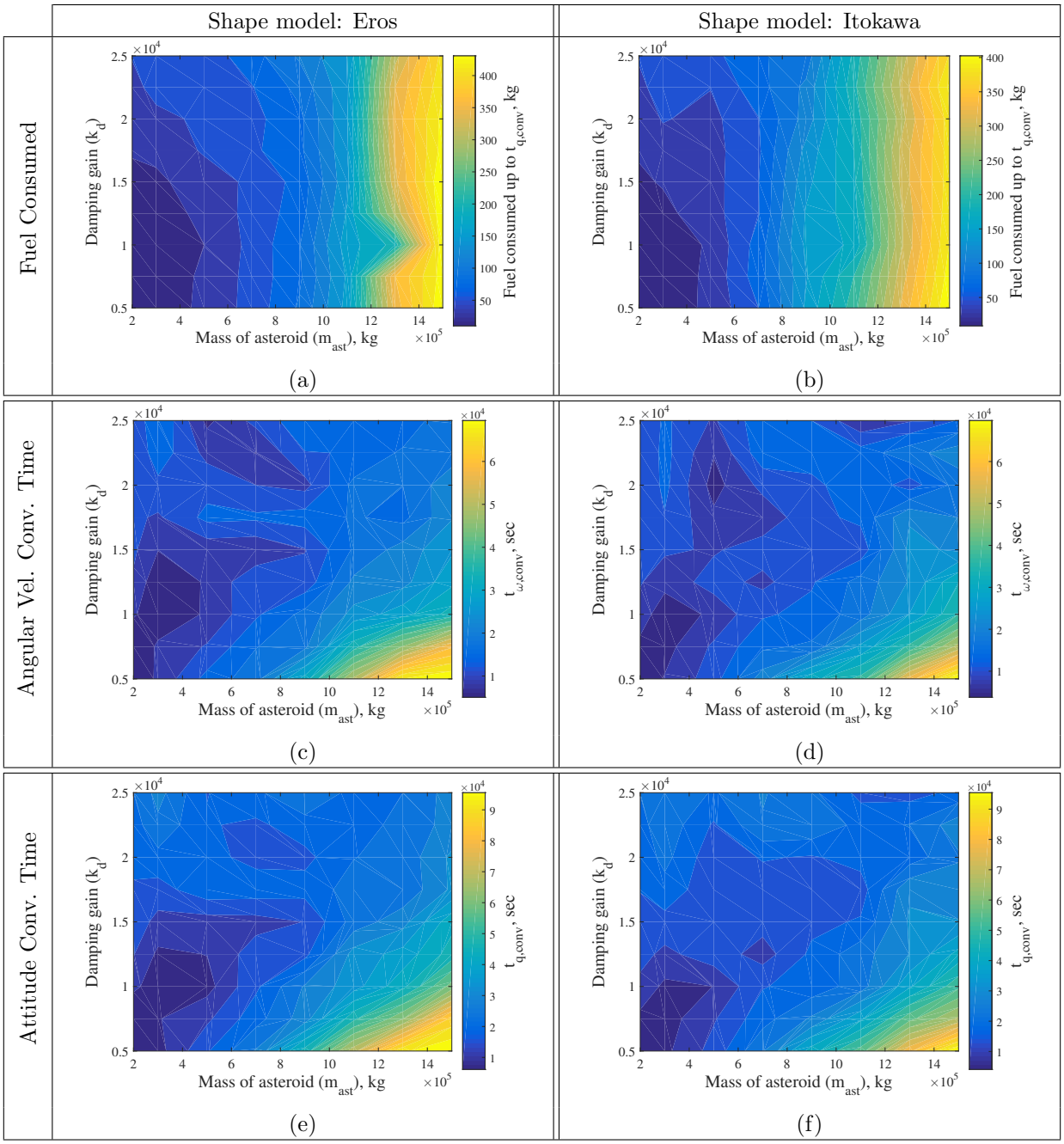

Figure 8: Sensitivity plots show the effect of the damping gain $\boldsymbol{K_d} = k_d\mathbf{I}$ on the convergence time of the angular velocity ($t_{\omega,\text{conv}}$), the convergence time of the attitude ($t_{q,\text{conv}}$), and the fuel consumed up to time $t_{q,\text{conv}}$ for the two shape models of Eros and Itokawa respectively.

VI. Conclusions

In this paper, we provide a detailed analysis of one of the main control challenges for the first ARM mission concept, namely despinning and three-axis stabilizing the tumbling asteroid and spacecraft combination after the asteroid has been captured by the ARM spacecraft. We first show that the control laws that use the knowledge of the dynamics of the system in the control law equation (a common characteristic of a nonlinear control law) experience a large resultant disturbance torque due to the modeling uncertainties. We then numerically compare the performance of three control laws: the robust nonlinear tracking control law Eq.

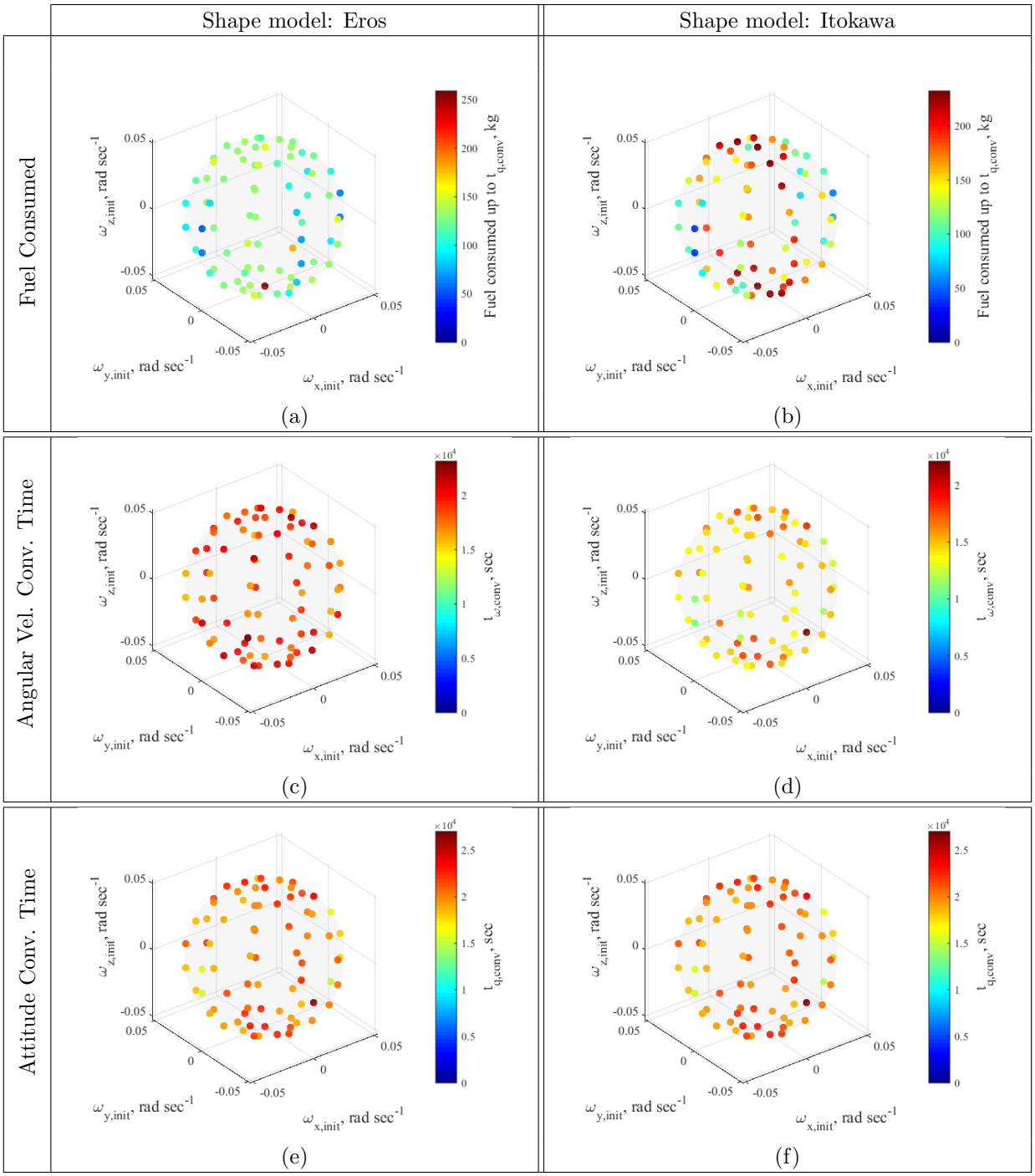

Figure 9: Sensitivity plots show the effect of the initial angular velocity $\boldsymbol{\omega}_{\text{initial}}$ on the convergence time of the angular velocity ($t_{\omega,\text{conv}}$), the convergence time of the attitude ($t_{q,\text{conv}}$), and the fuel consumed up to time $t_{q,\text{conv}}$ for the two shape models of Eros and Itokawa respectively, where the asteroid's mass is $m_{\text{ast}} = 1.1 \times 10^6$ kg and the asteroid's density is $\rho_{\text{ast}} = 1.9$ g cm^{-3}. All initial angular velocities are on the sphere with radius of 0.5 rpm.

(13), the adaptive nonlinear tracking control law Eqs. (27,28), and the derivative plus proportional-derivative (D+PD) control strategy Eqs. (30,37). We show that in the absence of measurement errors and under very small modeling uncertainties, which can be achieved using online system identification, the robust nonlinear tracking control law is the best strategy as it guarantees global exponential convergence to the fuel-optimal

reference trajectory, guarantees bounded tracking errors (finite-gain $\mathcal{L}_p$ stability and input-to-state stability) in the presence of disturbances, and consumes the least amount of fuel. We also show that a comparatively negligible amount of fuel ($\approx$ 1 kg) is needed for orientating the system to the desired attitude after the angular velocity of the system has stabilized.

On the other hand, in the presence of large modeling uncertainties, measurement errors, and actuator saturations, the D+PD control strategy is the best strategy for three-axis stabilizing the asteroid and spacecraft combination in the desired attitude orientation. With the help of sensitivity analysis, we show that the damping gain $k_d \approx 10^4$ is ideal for this ARM mission concept. We show that for all asteroids in the nominal range (i.e., the asteroid's mass is within 2.5-13 $\times 10^5$ kg, the asteroid's density is within 1.9-3.8 g cm^{-3}, and the asteroid's diameter is less than 15 m) and for all initial conditions (where the magnitude of the initial angular velocity is less than 0.5 rpm), the D+PD control strategy satisfies the transient and steady-state bounds and consumes less than 300 kg of fuel for despinning and three-axis stabilizing the asteroid and spacecraft combination. We also show that a comparatively negligible amount of fuel ($\approx$ 5 kg) is used by the proportional term in the D+PD control strategy for stabilizing the attitude of the asteroid and spacecraft combination.

Moreover, we show that the performance of the D+PD control strategy is sensitive to the magnitude of measurement errors in the angular velocity $\Delta\boldsymbol{\omega}$ and attitude $\Delta\boldsymbol{q}$. Hence, it is necessary that the sensors onboard the ARM spacecraft should ensure that the height of the power spectral density of these measurement errors should be less than the thresholds of $\mathcal{P}(\Delta\boldsymbol{\omega}) \leq 10^{-8}$ rad^2 sec^{-2} and $\mathcal{P}(\Delta\boldsymbol{q}) \leq 10^{-4}$. We also show that modeling uncertainties as high as 10% of their nominal values can be tolerated for the inertia tensor of the asteroid $\boldsymbol{J}_{\text{ast}}^{B_{CM}}$ and the distance from the base of the spacecraft to the center of mass of the combination $\boldsymbol{r}^{S_O/B_{CM}}$. Since the fuel consumed by the ARM spacecraft for this control problem is upper-bounded by 300 kg for all relevant situations, the total fuel that the ARM spacecraft needs to carry can be significantly reduced from the current capacity of 900 kg. The authors envisage that these guidelines can be used for improving the design of the ARM spacecraft.

Acknowledgments

The authors would like to thank A. Miguel San Martin and Gurkipal Singh for their valuable inputs. This research was supported by the Jet Propulsion Laboratory, California Institute of Technology, under a contract with the National Aeronautics and Space Administration.

References

[1]Brophy, J. R. and Friedman, L., "Returning an entire near-Earth asteroid in support of human exploration beyond low-Earth orbit," *IAF Global Exploration Conference*, Washington, D. C., May 2012.

[2]Tsuda, Y., Yoshikawa, M., Abe, M., Minamino, H., and Nakazawa, S., "System Design of the Hayabusa–2 Asteroid Sample Return Mission to 1999JU3," *Acta Astronautica*, Vol. 91, 2013, pp. 356–362.

[3]Harris, A., Barucci, M., Cano, J., Fitzsimmons, A., Fulchignoni, M., Green, S., Hestroffer, D., Lappas, V., Lork, W., Michel, P., Morrison, D., Payson, D., and Schaeffer, F., "The European Union Funded NEOSHIELD Project: A global Approach to Near-Earth Object Impact Threat Mitigation," *Acta Astronautica*, Vol. 90, No. 1, 2013, pp. 80–84.

[4]Glassmeier, K.-H., Boehnhardt, H., Koschny, D., Kührt, E., and Richter, I., "The Rosetta mission: flying towards the origin of the solar system," *Space Science Reviews*, Vol. 128, No. 1-4, 2007, pp. 1–21.

[5]Brophy, J. R., Gershman, R., Landau, D., Polk, J., Porter, C., Yeomans, D., Allen, C., Williams, W., and Asphaug, E., "Asteroid Return Mission Feasibility Study," *AIAA/ASME/SAE/ASEE Joint Propulsion Conf.*, San Diego, CA, July–August 2011.

[6]Brophy, J., Culick, F., and Friedman, L., "Asteroid Retrieval Feasibility Study," Tech. rep., Keck Institute for Space Studies, California Institute of Technology, Pasadena, CA, April 2012.

[7]Brophy, J. R., Friedman, L., and Culick, F., "Asteroid retrieval feasibility," *IEEE Aerospace Conference*, Big Sky, MT, March 2012, pp. 1–16.

[8]Brophy, J. R. and Oleson, S., "Spacecraft Conceptual Design for Returning Entire Near-Earth Asteroids," *AIAA/ASME/SAE/ASEE Joint Propulsion Conf.*, Atlanta, GA, July–August 2012.

[9]Mazanek, D. D., Brophy, J. R., and Merrill, R. G., "Asteroid Retrieval Mission Concept – Trailblazing Our Future in Space and Helping to Protect Us from Earth Impactors," *3rd IAA Planetary Defense Conf.*, Flagstaff, AZ, Apr. 2013.

[10]Merrill, R. G., Qu, M., Vavrina, M. A., Jones, C. A., and Englander, J., "Interplanetary Trajectory Design for the Asteroid Robotic Redirect Mission Alternate Approach Trade Study," *AIAA/AAS Astrodynamics Specialist Conf.*, San Diego, CA, Aug. 2014.

[11]"National Aeronautics and Space Administration, "NASA/Advanced Concepts Lab"," URL: http://www.nasa.gov/multimedia/imagegallery/image_feature_2520.html [cited January 12, 2015].

[12] "National Aeronautics and Space Administration, "NASA/Asteroid Initiative"," URL: http://www.nasa.gov/content/orion-docking-approach [cited January 12, 2015].

[13] Yárnoz, D. G., Sanchez, J. P., and McInnes, C. R., "Easily retrievable objects among the NEO population," *Celest Mech. Dyn. Astr.*, Vol. 116, June 2013, pp. 367–388.

[14] Strange, N. J., Landau, D., Longuski, J., and Chodas, P., "Identification of Retrievable Asteroids with the Tisserand Criterion," *AIAA/AAS Astrodynamics Specialist Conf.*, San Diego, CA, Aug. 2014.

[15] Landau, D., Dankanich, J., Strange, N., Bellerose, J., Llanos, P., and Tantardini, M., "Trajectories to nab a NEA (near-Earth asteroid)," *AAS/AIAA Spaceflight Mechanics Meeting*, Kauai, HI, Feb. 2013.

[16] Strange, N., Landau, D., McElrath, T., Lantoine, G., and Lam, T., "Overview of mission design for NASA Asteroid Redirect Robotic Mission concept," *Inter. Electric Propulsion Conf.*, Washington, D.C., Oct. 2013.

[17] Scheeres, D. J., "Close Proximity Operations for Implementing Mitigation Strategies," *Planetary Defense Conf.: Protecting Earth from Asteroids*, Orange County, CA, Feb. 2004.

[18] Biele, J., Ulamec, S., Jurado, E., Canalias, E., Blazquez, A., Martin, T., and Küppers, M., "Rosetta Comet Mission close proximity operations at comet 67P/Churyumov-Gerasimenko and landing Philae," *Lunar and Planetary Science Conf.*, Woodlands, TX, Mar. 2013.

[19] Takahashi, Y., *Gravity Field Characterization around Small Bodies*, Ph.D. thesis, University of Colorado at Boulder, 2013.

[20] Åström, K. J. and Eykhoff, P., "System Identification – A Survey," *Automatica*, Vol. 7, 1971, pp. 123–162.

[21] Giannakis, G. B. and Serpedin, E., "A bibliography on nonlinear system identification," *Signal Processing*, Vol. 81, No. 3, 2001, pp. 533–580.

[22] Adachi, S., Yamaguchi, I., Kida, T., Sekiguchi, T., Yamada, K., and Chida, Y., "On-orbit system identification experiments on Engineering Test Satellite-VI," *Control Engineering Practice*, Vol. 7, No. 7, 1999, pp. 831–841.

[23] Lee, A. Y. and Wertz, J. A., "In-flight estimation of the Cassini spacecraft's inertia tensor," *Journal of spacecraft and rockets*, Vol. 39, No. 1, 2002, pp. 153–155.

[24] Liu, Y., Kim, S. B., Chattopadhyay, A., and Doyle, D. T., "Application of System-Identification Techniquest to Health Monitoring of On-Orbit Satellite Boom Structures," *Journal of Spacecraft and Rockets*, Vol. 48, No. 4, 2011, pp. 589–598.

[25] Scheeres, D. J., "Close Proximity Dynamics and Control about Asteroids," *Amer. Control. Conf.*, Portland, OR, June 2014, pp. 1584–1598.

[26] Misra, G. and Sanyal, A., "Analysis of Orbit-Attitude Coupling of Spacecraft Near Small Solar System Bodies," *AIAA SciTech Guidance Navigation and Control Conf.*, Kissimmee, FL, Jan 2015, accepted.

[27] Bellei, G., Cano, J. L., and Sánchez, M., "Operational orbiting strategies about minor bodies," *21st International Symposium on Space Flight Dynamics ISSFD*, Toulouse,France, Oct. 2009.

[28] Grip, H. F., Ono, M., Balaram, J., Cameron, J., Jain, A., Kuo, C., Myint, S., and Quadrelli, M., "Modeling and simulation of asteroid retrieval using a flexible capture mechanism," *IEEE Aerospace Conf.*, Big Sky, MT, March 2014, pp. 1–14.

[29] Roithmayr, C. M., Shen, H., Jesick, M. C., and Cornelius, D. M., "Catching a Rolling Stone: Dynamics and Control of a Spacecraft and an Asteroid," *Proc. 3rd IAA Planetary Defense Conference*, Flagstaff, AZ, April 2013.

[30] Shen, H. and Roithmayr, C., "Co-Spin with Symmetry Axis Stabilization, and De-Spin for Asteroid Capture," *Amer. Control Conf.*, Portland, OR, June 2014, pp. 1599–1604.

[31] Luo, W., Chu, Y.-C., and Ling, K.-V., "Inverse Optimal Adaptive Control for Attitude Tracking of Spacecraft," *IEEE Trans. Autom. Control*, Vol. 50, No. 11, 2005, pp. 1639–1654.

[32] Ahmed, J., Coppola, V. T., and Bernstein, D., "Adaptive asymptotic tracking of spacecraft attitude motion with inertia matrix identification," *J. Guid. Control Dyn.*, Vol. 21, No. 5, 1998, pp. 684–691.

[33] Junkins, J. L., Akella, M. R., and Robinett, R. D., "Nonlinear adaptive control of spacecraft maneuvers," *J. Guid. Control Dyn.*, Vol. 20, No. 6, 1997, pp. 1104–1110.

[34] Chen, B.-S., Wu, C.-S., and Jan, Y.-W., "Adaptive fuzzy mixed H2/H∞ attitude control of spacecraft," *IEEE Trans. Aerospace Electron. Syst.*, Vol. 36, No. 4, 2000, pp. 1343–1359.

[35] Chung, S.-J., Bandyopadhyay, S., Chang, I., and Hadaegh, F. Y., "Phase synchronization control of complex networks of Lagrangian systems on adaptive digraphs," *Automatica*, Vol. 49, No. 5, May 2013, pp. 1148–1161.

[36] Crassidis, J. L. and Markley, F. L., "Sliding mode control using modified Rodrigues parameters," *J. Guid. Control Dyn.*, Vol. 19, No. 6, 1996, pp. 1381–1383.

[37] Yeh, F.-K., "Sliding-mode adaptive attitude controller design for spacecrafts with thrusters," *IET Control Theory Appl.*, Vol. 4, No. 7, 2010, pp. 1254–1264.

[38] Pukdeboon, C. and Zinober, A. S. I., "Optimal sliding mode controllers for attitude tracking of spacecraft," *IEEE Control Applicat. & Intelligent Control*, St. Petersburg, Russia, 2009, pp. 1708–1713.

[39] Zhou, K., Doyle, J. C., and Glover, K., *Robust and optimal control*, Vol. 40, Prentice Hall New Jersey, 1996.

[40] Kang, W., "Nonlinear H∞ control and its application to rigid spacecraft," *IEEE Trans. Autom. Control*, Vol. 40, No. 7, 1995, pp. 1281–1285.

[41] Wie, B. and Barba, P. M., "Quaternion feedback for spacecraft large angle maneuvers," *J. Guid. Control Dyn.*, Vol. 8, No. 3, 1985, pp. 360–365.

[42] Tsiotras, P., "Stabilization and optimality results for the attitude control problem," *J. Guid. Control Dyn.*, Vol. 19, No. 4, 1996, pp. 772–779.

[43] Song, Y. D. and Cai, W., "Quaternion observer-based model-independent attitude tracking control of spacecraft," *J. Guid. Control Dyn.*, Vol. 32, No. 5, 2009, pp. 1476–1482.

[44] Weiss, A., Kolmanovsky, I., Bernstein, D. S., and Sanyal, A., "Inertia-Free Spacecraft Attitude Control Using Reaction Wheels," *J. Guid. Control Dyn.*, Vol. 36, No. 5, 2013, pp. 1425–1439.

[45]Gaskell, R. W., "Gaskell Eros shape model V1.0. NEAR-A-MSI-5-EROSSHAPE-V1.0." Tech. rep., NASA Planetary Data System, 2008.

[46]Gaskell, R., Saito, J., Ishiguro, M., Kubota, T., Hashimoto, T., Hirata, N., Abe, S., Barnouin-Jha, O., and Scheeres, D., "Gaskell Itokawa shape model V1.0. HAY-A-AMICA-5-ITOKAWASHAPE-V1.0." Tech. rep., NASA Planetary Data System, 2008.

[47]Sidi, M. J., *Spacecraft Dynamics and Control*, Cambridge Univ. Press, Cambridge, U.K., 1997.

[48]Wie, B., *Space vehicle dynamics and control*, AIAA, 1998.

[49]Chaturvedi, N. A., Sanyal, A. K., and McClamroch, N. H., "Rigid–Body Attitude Control," *IEEE Control Syst. Mag.*, Vol. 31, No. 3, 2011, pp. 30–51.

[50]Schaub, H. and Junkins, J. L., "Stereographic Orientation Parameters for Attitude Dynamics: A Generalization of the Rodrigues Parameters," *Journal of the Astronautical Sciences*, Vol. 44, No. 1, Jan.–Mar. 1996, pp. 1–19.

[51]Chung, S.-J., Ahsun, U., and Slotine, J.-J. E., "Application of Synchronization to Formation Flying Spacecraft: Lagrangian Approach," *J. Guid. Control Dyn.*, Vol. 32, No. 2, Mar.-Apr. 2009, pp. 512–526.

[52]Slotine, J.-J. E. and Li, W., *Applied Nonlinear Control*, Vol. 199, Prentice-Hall Englewood Cliffs, NJ, 1991.

[53]Khalil, H. K., *Nonlinear Systems*, Macmillan Pub. Co., New York, 1992.

[54]Krstic, M. and Tsiotras, P., "Inverse optimal stabilization of a rigid spacecraft," *IEEE Trans. Autom. Control*, Vol. 44, No. 5, 1999, pp. 1042–1049.

[55]Sharma, R. and Tewari, A., "Optimal nonlinear tracking of spacecraft attitude maneuvers," *IEEE Trans. Control Systems Technology*, Vol. 12, No. 5, 2004, pp. 677–682.

[56]Schaub, H., Junkins, J. L., and Robinett, R. D., "New penalty functions and optimal control formulation for spacecraft attitude control problems," *J. Guid. Control Dyn.*, Vol. 20, No. 3, 1997, pp. 428–434.

[57]Garg, D., Patterson, M., Hager, W. W., Rao, A. V., Benson, D. A., and Huntington, G. T., "A unified framework for the numerical solution of optimal control problems using pseudospectral methods," *Automatica*, Vol. 46, No. 11, 2010, pp. 1843–1851.

[58]Chung, S.-J. and Slotine, J. J. E., "Cooperative robot control and concurrent synchronization of Lagrangian systems," *IEEE Trans. Robotics*, Vol. 25, No. 3, 2009, pp. 686–700.

[59]Rao, A. V., Benson, D. A., Darby, C. L., Patterson, M. A., Francolin, C., Sanders, I., and Huntington, G. T., "GPOPS: A MATLAB Software for Solving Multiple-Phase Optimal Control Problems Using the Gauss Pseudospectral Method," *ACM Trans. Mathematical Software*, Vol. 37, No. 2, March-April 2010, pp. 39, Article 22.

[60]Patterson, M. A. and Rao, A. V., "GPOPS-II: A MATLAB Software for Solving Multiple-Phase Optimal Control Problems Using hp-Adaptive Gaussian Quadrature Collocation Methods and Sparse Nonlinear Programming," *ACM Transactions on Mathematical Software*, Dec. 2013.